



# Waves in the Earth's core. II. Magneto–Coriolis modes

**Journal Article****Author(s):**

[Luo, Jiawen](#) ; [Marti, Philippe David](#) ; Jackson, Andrew

**Publication date:**

2022-05-25

**Permanent link:**

<https://doi.org/https://doi.org/10.3929/ethz-b-000548469>

**Rights / license:**

[Creative Commons Attribution 4.0 International](#)

**Originally published in:**

Proceedings of the Royal Society A: Mathematical, Physical and Engineering Sciences 478(2261), <https://doi.org/10.1098/rspa.2022.0108>

**Funding acknowledgement:**

- Unravelling Earth's magnetic history and processes UEMHP ()
- Developing the next generation of inviscid, inertialess dynamo models in spheres and spherical shells ()

## Research



**Cite this article:** Luo J, Marti P, Jackson A.

2022 Waves in the Earth's core. II.

Magneto–Coriolis modes. *Proc. R. Soc. A* **478**:

20220108.

<https://doi.org/10.1098/rspa.2022.0108>

Received: 11 February 2022

Accepted: 7 April 2022

**Subject Areas:**

geophysics

**Keywords:**

magneto–Coriolis normal mode,

magnetostrophic limit

**Author for correspondence:**

Jiawen Luo

e-mail: [jiawen.luo@erdw.ethz.ch](mailto:jiawen.luo@erdw.ethz.ch)

Electronic supplementary material is available online at <https://doi.org/10.6084/m9.figshare.c.5958959>.

# Waves in the Earth's core. II. Magneto–Coriolis modes

Jiawen Luo, Philippe Marti and Andrew Jackson

Institut für Geophysik, ETH Zürich, Sonneggstrasse 5, Zürich 8092, Switzerland

JL, 0000-0003-4736-1404

We investigate the normal modes of a rapidly rotating, electrically conducting, inviscid fluid sphere in the presence of a background magnetic field. Neglecting the fast modes that are essentially slightly modified inertial waves, we focus on the slower branch of modes traditionally called magneto–Coriolis (MC) modes. We focus on the magnetostrophic limit, an approximation that neglects the fluid inertia for these modes by setting the magnetic Rossby number  $E_\eta$  equal to zero, converting the momentum equation from a prognostic to a diagnostic equation. In contrast to a local analysis and contrary to previous assertions, this inertialess-inviscid double limit is perfectly well behaved and shows that  $E_\eta \rightarrow 0$  and  $E_\eta = 0$  are essentially identical. With applied axisymmetric background fields, we find the modes are critically damped, with decay rates greater than or equal to the eigenfrequency, in contrast to the local theory. We find evidence for both eastward and westward propagating columnar modes, in contradiction of commonly perceived wisdom. The results bode well for numerical time integrations based on the magnetostrophic approximation, which is highly suited to the core of the Earth and holds the potential for more realistic solutions of the dynamo equations.

## 1. Introduction

Rapidly rotating, electrically conducting, fluid cores exist in the rocky planets, in gas giants and in stars. They are often the seat of processes leading to magnetic field generation (the dynamo process), taking place on time scales in excess of  $10^5$  years. On shorter time scales, the systems can support different types of oscillations or normal modes.

Such modes have been observed in profusion in the non-magnetic contexts of oceans and atmospheres; in the magnetic context there is but one unequivocal observation of such a mode, namely in the core of the Earth by [1]. This observation is of a particular mode that is almost perfectly geostrophic ( $z$ -invariant, where  $z$  is the axis of rotation) and zonal. The question remains open as to whether other modes are strongly excited in the Earth or in other planets and stellar interiors. To gain insight into the types of modes that may occur, and into their eigenfrequencies, it is typical to consider the behaviour of the system in the presence of a background magnetic field. The form of the magnetic field is generally unknown, so particular forms of field can be taken at will and subsequent behaviour deduced. This is precisely the approach adopted here. Of course, simplicity is paramount and thus we consider behaviour in the presence of applied axisymmetric fields. It is possible that behaviour could be different for more exotic background fields, but the calculations performed here, which can be carried out in exactly the Earth-like regime, would no longer be computationally tractable. A vast literature exists on the theory of modes starting with [2–5]; for a thorough review, we refer the reader to [6].

Our motivation for studying modes of these systems is not because of the interest in the modes *per se*; indeed, we consider it reasonably unlikely that specific eigenmodes can be excited such that they become the dominant feature of the physical system, particularly the Earth's core. Our motivation is more general: the behaviour of normal modes can have severe repercussions for numerical time integrations of the governing equations, and it is our personal interest in the generation mechanism of the Earth's dynamo that motivates us to clarify the normal modes of the system more thoroughly than has been done before.

Reviews of waves under the influence of rapid rotation and magnetic fields are given in [6,7]. Because the effect of dissipation is to cause wave decay, most analyses tend to favour the ideal or diffusionless limit, in which the effects of Ohmic decay (finite electrical conductivity) are discounted. In this paper, we defer from this approximation and take into account realistic diffusion, finding that it plays a pivotal role.

As is well known [8,9], an inviscid fluid subject to rapid rotation at angular velocity  $\Omega$  can support normal modes termed *inertial modes* with time variation  $e^{i\omega t}$ , whose frequencies  $\omega$  obey  $|\omega| \leq 2\Omega$ . We shall see that in the more general setting in which the fluid is electrically conducting and immersed in a background magnetic field, these modes endure essentially unaltered. The presence of such waves has huge repercussions for numerical integrations of the equations of rotating magnetohydrodynamics (MHD): such waves must be resolved by explicit schemes (overwhelmingly the most common time integration schemes), and thus impose prohibitively small time-step limits on the calculation. For example, consider a self-excited dynamo calculation whose aim is to demonstrate sustained magnetic field creation in a certain physical scenario over a few magnetic diffusion time scales. If time is measured in magnetic diffusion times  $\tau = L^2/\eta$  where  $\eta$  is the magnetic diffusivity and  $L$  is a length scale of the system, the non-dimensional time scale of the fastest waves is  $2\pi/(2\tau\Omega)$ . Defining the magnetic Rossby number as

$$E_\eta = \frac{\eta}{2\Omega L^2}, \quad (1.1)$$

we see that the period of the inertial waves is  $2\pi E_\eta$ . In the Earth's core  $E_\eta \sim 10^{-9}$  and thus an immense number of time steps must be taken per diffusion time if one wishes to replicate the Earth's true parameter regime. For this reason, simulations compromise quite strongly on their choice of control parameters, losing realism.

There are differences of opinion on the role of inertial waves in the geodynamo (as reviewed in [10]): some proponents claim that they are at the heart of the regeneration process [11–17], while we take an opposing view and developed this work in support of our dynamo calculations in which inertial waves play no part.

The idea of filtering inertial waves from the system has a long history. In a classic work, Taylor [18] realized that the smallness of the inertial and viscous terms in the equation of fluid motion could be used to advantage: when set to zero the fluid motion is governed by a diagnostic (rather than prognostic) equation and becomes a slave of the temperature field and magnetic field, both

of which are subject to time-evolution equations. In neglecting inertia ( $\partial_t \mathbf{u}$ ), the equations of motion can no longer support the branch of waves that are very slightly modified inertial waves. Ignorance of kinematic viscosity  $\nu$  dispenses with the need to resolve the viscous boundary layer that can form adjacent to a solid interface with width  $\sqrt{E}$  where  $E$  is the Ekman number defined as

$$E = \frac{\nu}{2\Omega L^2}, \quad (1.2)$$

with an exceedingly small value of  $10^{-15}$  in the Earth.

A serious blow was dealt to the idea by the well-known work of [19] who showed that in an infinite domain, by ignoring inertia and viscosity, small scale rapidly oscillating MHD waves develop and are expected to cause numerical instabilities. This analysis has been restated in several other works, for example [20–22], and has contributed to a community timidity towards this approximation. A recent discussion of this point can be found in [23]. For clarity of exposition, we repeat here the classic development that leads to conclusions that stem from a local analysis.

We consider a uniform background field  $\mathbf{B}_0$  and quiescent  $\mathbf{U}_0 = 0$  fluid in an infinite domain with the plane wave ansatz. For magnetic fields  $\mathbf{b}$  and velocities  $\mathbf{u}$

$$\mathbf{b} = \tilde{\mathbf{b}} e^{i\mathbf{k}\cdot\mathbf{r} + \tilde{\omega}t} \quad \text{and} \quad \mathbf{u} = \tilde{\mathbf{u}} e^{i\mathbf{k}\cdot\mathbf{r} + \tilde{\omega}t}, \quad (1.3)$$

where  $\tilde{\omega}$  is the complex eigenfrequency,  $\mathbf{k}$  is the wavenumber and  $\mathbf{r}$  is the position vector. Substituting (1.3) into the linearized equations of motion and magnetic induction, to be discussed in §2, yields a dispersion relation

$$-(E_\eta \tilde{\omega} + Ek^2)(\tilde{\omega} + k^2) - \omega_M^2 \pm i\omega_C(\tilde{\omega} + k^2) = 0, \quad (1.4)$$

where  $k = |\mathbf{k}|$  and

$$\omega_M = \mathbf{k} \cdot \mathbf{B}_0 \quad \text{and} \quad \omega_C = \frac{(\mathbf{k} \cdot \hat{\mathbf{z}})}{k}. \quad (1.5)$$

The Ekman and magnetic Rossby numbers were introduced in (1.2) and (1.1), respectively. While recognizing that there is no clear length scale in an infinite medium, an arbitrary choice for  $L$  can be made such that  $E$  and  $E_\eta$  are Earth-like; the conclusions below hold nevertheless.

In the case of magnetostrophy, i.e. both  $E_\eta$  and  $E$  taken to be zero (note that now (1.4) is linear), we obtain

$$\tilde{\omega} = \mp i \frac{\omega_M^2}{\omega_C} - k^2. \quad (1.6)$$

Assume the angle between  $\mathbf{k}$  and  $\hat{\mathbf{z}}$  is  $\theta$ , between  $\mathbf{k}$  and  $\mathbf{B}_0$  is  $\gamma$ . Thus,

$$\omega_C = \cos \theta \quad \text{and} \quad \omega_M = k|\mathbf{B}_0| \cos \gamma. \quad (1.7)$$

Then (1.6) can be rewritten as

$$\omega = k^2 \left[ \mp i \frac{|\mathbf{B}_0|^2 \cos^2 \gamma}{\cos \theta} - 1 \right], \quad (1.8)$$

and we note that the waves are dispersive [2,3]. Suppose  $|\mathbf{B}_0|$  is  $O(1)$  and  $\mathbf{B}_0$  is not in alignment with  $\hat{\mathbf{z}}$ . When  $\mathbf{k}$  approaches perpendicularity to  $\hat{\mathbf{z}}$ ,  $\omega_C = \cos \theta$  tends to zero. Equation (1.8) indicates that such a mode can have a frequency much larger than its damping rate, despite the fact that both of them are proportional to  $k^2$ . This observation leads to the conclusion that magnetostrophy in an unbounded domain results in an even stiffer system than before by neglecting viscosity and filtering out fast inertial waves [19].

One of the primary purposes of this paper is to show that the doom cast over the magnetostrophic approximation is unwarranted. We find that  $E_\eta \rightarrow 0$  is essentially equivalent to  $E_\eta = 0$ ; the latter has the tremendous advantage that there are no unwanted inertial waves in the system, untrue of the former. In comparison with the local analysis, not only do we *not* find modes whose decay rate is significantly small compared with its frequency, we also show that it

is the simplification of the local analysis that does not capture the true modes that exist in a closed spherical volume.

The Earth's magnetic field is observed to have drifted in a westerly direction over the last few centuries, and this zeroth-order datum has been the motivation for numerous studies. Of major importance was the development of Hide [24] who showed that when a columnar ansatz (invariance of components of  $\mathbf{u}$  perpendicular to  $z$ ) is taken, it is expected that slow modes travel west and the fast branch travels east, clearly of relevance to the secular variation; the result has been reproduced many times e.g. [25, §8.09.2.2.2] or [26]. Hori and collaborators [27,28] studied the normal mode system in the ideal limit ( $\eta = 0$ ) but with finite  $E_\eta$  and found the dispersion relation for magnetic Rossby waves. Adopting a columnar ansatz for the flow, they reproduce the work of [24] in finding that the slow modes all propagate westwards. Through the explicitly soluble example of Malkus [29], this division of columnar Rossby wave propagation direction has reached the level of folk law. We show explicitly that this perceived wisdom is not secure and demonstrate both eastward and westward propagation directions.

We have mentioned the preponderance of studies that take the ideal limit; one must question this limit for a core such as that of the Earth, and indeed we find in a companion paper [30] that the presence of magnetic diffusion is essential for the existence of torsional modes in an axisymmetric background field. It is the purpose of the present paper to investigate modes whose periods may be (but are not necessarily) longer than those of the torsional oscillations (TOs), thus rendering the inclusion of diffusion of paramount importance. We remind the reader that diffusion of momentum (through viscosity) is neglected throughout our paper, as is befitting of a physical system with a small magnetic Prandtl number and with rapid rotation.

A notable exception to the diffusionless studies is that of Schmitt [31]. He quotes attenuation rates for a selection of MC modes, albeit calculated at the relatively high values of the Ekman number  $E \sim 10^{-4}$ , with  $0 \leq E_\eta \leq 10^{-3}$  so that often it is viscosity rather than magnetic diffusivity that is dominant, not really the scenario envisaged in the Earth. In [32], in another three-dimensional study, it was found that magnetic diffusion plays an important role when the Elsasser number  $\Lambda \ll 1$  (i.e. magnetic forces are weak compared with Coriolis forces), when the normal modes become so-called quasi-free decay (QFD) modes. In the  $\Lambda \ll 1$  limit, [32] found both eastward and westward propagating modes, but these modes are decaying rapidly such that the epithet 'propagating' is questionable.

The arrangement of the paper is as follows: in §2, we introduce the governing equations and discuss the magnetostrophic limit in a full sphere. The numerical methodology is described in §3. In §4, we re-study the Malkus background field, this time in the presence of magnetic diffusion; results for a series of three background fields are also reported. In the Discussion (§5), we report on several aspects of our results, including the appropriateness of the magnetostrophic limit and the propagation direction of columnar modes.

## 2. Governing equations

### (a) Magnetohydrodynamic equations

The governing equations for the incompressible flow  $\mathbf{u}$  and magnetic field  $\mathbf{B}$  in a rapidly rotating sphere are given by

$$\rho(\partial_t \mathbf{u} + \mathbf{u} \cdot \nabla \mathbf{u} + 2\boldsymbol{\Omega} \times \mathbf{u}) = -\nabla p + \frac{1}{\mu_0}(\nabla \times \mathbf{B}) \times \mathbf{B} + \rho\nu \nabla^2 \mathbf{u} \quad (2.1)$$

and

$$\partial_t \mathbf{B} = \nabla \times (\mathbf{u} \times \mathbf{B}) + \eta \nabla^2 \mathbf{B}, \quad (2.2)$$

where  $\boldsymbol{\Omega}$  is the rotation rate pointing in the  $\hat{z}$  direction,  $\rho$  is the density,  $\mu_0$  is magnetic permeability of free space and  $p$  is the pressure.  $\nu$  and  $\eta$  are the kinematic viscosity and magnetic diffusivity, respectively, both assumed to be constant in the whole sphere.

In this study, we consider linear perturbations of the system with respect to a background magnetic field  $\mathbf{B}_0$  and a zero background flow, i.e.  $\mathbf{U}_0 = 0$ . We recognize that frequencies in particular can be altered by the presence of a thermal or magnetic wind leading to  $\mathbf{U}_0 \neq 0$  but neglect this complication. By taking the sphere radius  $R$ ,  $R^2/\eta$  and  $(2\Omega\mu_0\rho\eta)^{1/2}$  as unit of the length, time and magnetic field, respectively, and linearizing (2.1) and (2.2), we obtain the linearized non-dimensional equations

$$E_\eta \partial_t \mathbf{u} + \hat{\mathbf{z}} \times \mathbf{u} = -\nabla p + \Lambda^{1/2} [(\nabla \times \mathbf{b}) \times \mathbf{B}_0 + (\nabla \times \mathbf{B}_0) \times \mathbf{b}] + E \nabla^2 \mathbf{u} \quad (2.3)$$

and

$$\partial_t \mathbf{b} = \Lambda^{1/2} \nabla \times (\mathbf{u} \times \mathbf{B}_0) + \nabla^2 \mathbf{b}. \quad (2.4)$$

In the above equations,  $\mathbf{u}$  and  $\mathbf{b}$  are the non-dimensional perturbations of the flow and the magnetic field. Non-dimensional parameters are the Ekman, magnetic Rossby and Elsasser number, defined to be

$$E = \frac{\nu}{2\Omega R^2}, \quad E_\eta = \frac{\eta}{2\Omega R^2} \quad \text{and} \quad \Lambda = \frac{\mathcal{B}^2}{2\Omega\mu_0\rho\eta}, \quad (2.5)$$

in which  $\mathcal{B}$  is a typical strength of the background magnetic field. The Ekman number  $E$  measures the relative strength between the viscous force and Coriolis force, and the magnetic Rossby number  $E_\eta$  measures the ratio between the periods of inertial waves and the magnetic diffusion time scale. We have mentioned that these numbers are of  $O(10^{-15})$  and  $O(10^{-9})$  for the Earth. The Elsasser number  $\Lambda$  determines the strength of the background magnetic field, and is estimated to be  $O(1) \sim O(10)$  for the Earth.

The miniscule value of the Ekman number leads to the expectation that viscous dissipation plays an insignificant role in the geodynamo problem. More specifically, the small magnetic Prandtl number  $Pm = E/E_\eta = \nu/\eta \sim O(10^{-6})$  suggests that magnetic diffusion is the dominant diffusive effect in the Earth's core for similar length scales. This motivates our choice of the magnetic diffusion time  $R^2/\eta$  as the time scale. We shall thus neglect  $E \nabla^2 \mathbf{u}$  in all the following eigenmode calculations.

## (b) The magnetostrophic limit

Recalling that we take  $E = 0$ , J. B. Taylor [18] also considered setting the other small parameter  $E_\eta$  to be zero at the same time and the resulting force balance was later termed as *magnetostrophy* by [33], with the generalization that a buoyancy force can also be present in the formulae. In our linearized, convection-free scenario, the magnetostrophic limit is described by

$$\hat{\mathbf{z}} \times \mathbf{u} = -\nabla p + \Lambda^{1/2} [(\nabla \times \mathbf{b}) \times \mathbf{B}_0 + (\nabla \times \mathbf{B}_0) \times \mathbf{b}]. \quad (2.6)$$

[18] proved that (2.6) has a unique solution for  $\mathbf{u}$  with non-penetration boundary conditions if and only if the Lorentz force  $\mathbf{F}_L$  satisfies a solvability condition, called Taylor's constraint

$$\langle \mathbf{F}_L \cdot \hat{\boldsymbol{\phi}} \rangle = 0, \quad (2.7)$$

where  $\langle \cdot \rangle$  is the cylinder average over geostrophic cylinders  $C(s)$  surrounding the rotation axis at cylindrical radius  $s$ . Magnetic fields satisfying this condition are called Taylor state magnetic fields. This condition is automatically satisfied for an axisymmetric background field  $\mathbf{B}_0$  and non-axisymmetric perturbations  $\mathbf{b}$ . Thus (2.6) and (2.4) form a linear eigensystem for  $\mathbf{b}$  for azimuthal wavenumber  $m \neq 0$  in the magnetostrophic limit. For  $m = 0$ , (2.7) is generally not satisfied and [18] realized that perturbations from a Taylor state field would be in the form of motions on geostrophic cylinders, named as TOs. Dissipative TOs have been treated in a preceding paper [30].

Potential problems with the inviscid, inertialess approximation were discussed in the Introduction for an infinite space. In a whole sphere, a special choice of

$$\mathbf{B}_0 = s\hat{\phi}, \quad (2.8)$$

known as the Malkus field [29], allows analytical solution of the diffusion-less version of (2.3) and (2.4). The analytical solution for the fast and slow branches is presented in appendix A and (A 5) exactly gives the dispersion relation. By neglecting the inertial term, we essentially filter out the fast inertial branch with frequencies  $\omega_i$ . The slow branch of interest has frequency (A 7), which we here reprise

$$\omega \approx -\frac{2\Lambda m(m - \omega_i)}{\omega_i}, \quad (2.9)$$

attention to which was drawn by [34]. Note that the inertial frequency  $\omega_i$  tends to zero for increasingly complex modes. These inertial modes are known to have columnar structures, and are usually referred to as quasi-geostrophic (QG) inertial modes ([35]; [9]). Equation (4.5) of [35] gives an approximation for the QG inertial modes' frequencies, parametrized by  $k_s$ ,

$$\omega_i^{(k_s)} \approx -\frac{2}{m+2} \left( \sqrt{1 + \frac{m(m+2)}{k_s(2k_s+2m+1)}} - 1 \right) \approx -\frac{m}{k_s(2k_s+2m+1)}, \quad (2.10)$$

in which  $k_s$  can be understood as the wavenumber in the cylindrical radial direction. The second approximation in (2.10) assumes a large  $k_s$ . Estimation (2.10) and (2.9) lead to the frequency of the slow branch being  $O(k_s^2)$ . This seems to reinstate the conclusion of [19]. However, note that if magnetic dissipation is considered, the large  $k_s$  modes are likely to be strongly damped by the dissipation at a rate of  $O(k_s^2)$  too. This contrasts with the plane wave case, for which an infinite frequency is allowed with only a small dissipation rate. In §5, we will show that in a whole sphere, as a bounded domain, the singular behaviour of the plane wave case is not present due to the assistance of magnetic diffusion. Magnetic modes with high frequency tend to have decay rates comparable with or greater than their frequencies, at least when the background field is axisymmetric. We also find that taking  $E_\eta \rightarrow 0$  is equivalent to setting  $E_\eta = 0$  in terms of the slow MC modes.

### 3. Numerical methodology

#### (a) Construction of matrices

We decompose  $\mathbf{u}$  and  $\mathbf{b}$  into its toroidal and poloidal parts using their divergence-free properties

$$\mathbf{u} = \nabla \times \nabla \times \mathcal{S}_u(t, r, \theta, \phi)\mathbf{r} + \nabla \times \mathcal{T}_u(t, r, \theta, \phi)\mathbf{r} \quad (3.1)$$

and

$$\mathbf{b} = \nabla \times \nabla \times \mathcal{S}_b(t, r, \theta, \phi)\mathbf{r} + \nabla \times \mathcal{T}_b(t, r, \theta, \phi)\mathbf{r}.$$

We work in both spherical polar  $(r, \theta, \phi)$  and cylindrical  $(s, \phi, z)$  coordinates. As in the preceding paper [30], equations (2.3) and (2.4) are reduced to scalar equations for the toroidal and poloidal scalars. We make the ansatz that  $\mathcal{T}_u$ ,  $\mathcal{S}_u$ ,  $\mathcal{T}_b$  and  $\mathcal{S}_b$  have time dependence in the form of  $e^{\tilde{\omega}t}$ , in which  $\tilde{\omega}$  is the eigenvalue which can be decomposed as

$$\tilde{\omega} = -\sigma + i\omega. \quad (3.2)$$

$\omega$  is the oscillation frequency and  $\sigma$  is the decay rate. In our notation, for azimuthal wavenumber  $m > 0$ ,  $\omega > (<)0$  means westward (eastward) waves. As only axisymmetric  $\mathbf{B}_0$  is considered, the system becomes independent for each  $m$ . At a single  $m$ , these scalars are further expanded in the tangential direction by fully normalized complex spherical harmonics  $Y_l^m(\theta, \phi)$  with order  $l \leq L + m - 1$  and in radial direction by Jones–Worland (J-W) polynomials  $W_n^l(r)$  [36–40] up to order  $N$ . The J-W basis function guarantees infinite differentiability of all the scalars and resolves the artificial singularity occurring at centre of the sphere in spherical coordinates [41]. For inviscid flows considered in this work, we use a non-penetration boundary condition for  $\mathbf{u}$ ,

i.e.  $\mathbf{u} \cdot \hat{\mathbf{n}} = 0$ , and an insulating condition for the magnetic field perturbation  $\mathbf{b}$ . The matrices are then constructed using the method described in [30]. For more technical details about the matrix construction and eigenvalue computation, we refer the reader to [30].

## (b) Symmetry

First, since every background field considered is axisymmetric, there is no coupling between different azimuthal wavenumbers for eigenmodes of the system. Second, we consider the symmetry separation with respect to the equator, see [42] for more discussion on the symmetry property. We denote a vector or scalar field with symmetry **QP/DP** if it is symmetric/antisymmetric with respect to the equator. Equatorial parity of  $\mathbf{B}_0$  (if exists) defines independent symmetry groups of  $\mathbf{u}$  and  $\mathbf{b}$ . A **QP**  $\mathbf{B}_0$  allows  $\mathbf{u}$  and  $\mathbf{b}$  to be both **DP** or **QP**, while a **DP**  $\mathbf{B}_0$  leads to  $\mathbf{u}$  and  $\mathbf{b}$  of opposite parities. To avoid confusion, we shall denote the symmetry group of the eigenmode  $(\mathbf{u}, \mathbf{b})$  according to that of  $\mathbf{b}$ . For example, in the case that  $\mathbf{B}_0$  is **DP**,  $\mathbf{u}$  is **DP** and  $\mathbf{b}$  is **QP**, we shall refer to it as the **QP** symmetry group.

## 4. Results

### (a) Background fields

We consider the Malkus field (2.8) and additionally three other configurations of  $\mathbf{B}_0$ , two of opposite equatorial parities, denoted by T1 and S1, and one of mixed equatorial parities, denoted by T1S1. All latter three satisfy the insulating boundary condition. T1 is an  $l = 1$  toroidal field with the first simplest mode of a Galerkin expansion in  $r$

$$\mathbf{B}_0 = \frac{3\sqrt{3}}{2} r(1 - r^2) \sin \theta \hat{\boldsymbol{\phi}}, \quad (4.1)$$

thus it is of **QP** parity. S1 is the  $l = 1$  poloidal field with the simplest radial mode

$$\begin{aligned} \mathbf{B}_0 &= \frac{1}{10} \nabla \times \nabla \times r(5 - 3r^2) \cos \theta \mathbf{r} \\ &= \frac{1}{5} ((5 - 3r^2) \cos \theta \hat{\mathbf{r}} + (-5 + 6r^2) \sin \theta \hat{\boldsymbol{\theta}}). \end{aligned} \quad (4.2)$$

S1 is by definition of **DP** parity. These two simple fields are normalized such that  $\max |\mathbf{B}_0| = 1$  in the sphere. In terms of the energy  $\int_V \mathbf{B}_0^2 d^3x$ , these have values about 1.4 for T1 and 1.1 for S1. We also consider a mixture of these two modes, denoted by T1S1,

$$\mathbf{B}_0 = \frac{3}{8} \sqrt{\frac{105}{2\pi}} r(1 - r^2) \sin \theta \hat{\boldsymbol{\phi}} + \frac{1}{4} \sqrt{\frac{7}{23}} \nabla \times \nabla \times r(5 - 3r^2) \cos \theta \mathbf{r}. \quad (4.3)$$

The ratio between the toroidal and poloidal components is chosen such that they contribute equally to the magnetic energy, and  $\int_V \mathbf{B}_0^2 d^3x = 1$  in total. We remark that all three background fields are Taylor states by symmetry [43], so the set-up is fully consistent in taking the magnetostrophic limit. The equatorial parity of T1 and S1 allows a separation of symmetry by the discussion in §3b, while eigenmodes of the mixed T1S1 configuration generally have components from both **DP** and **QP** parities. In the following, we first compute eigenvalues at low spatial resolutions with relatively large choices of  $E_\eta$ , e.g.  $10^{-4}$  and  $10^{-6}$ , and also  $E_\eta = 0$  to illustrate the distribution of the normal mode eigenvalues. Subsequent computations of specific modes that occur in the discussion are all computed with  $E_\eta = 10^{-9}$  at a higher spatial resolution. We have set  $\Lambda = 1$  for most of the calculations. To aid navigation through the various modes that we describe, we provide in table 1 an aide-mémoire with characteristics of the modes, where, for example T1-E1 is eigenmode E1 for field T1.

**Table 1.** Characteristics of the modes described. The eigenvalue is  $\tilde{\omega}$ , azimuthal wavenumber is  $m$ , kinetic to magnetic energy ratio is  $E_k/E_m$ , parity is that of the  $\mathbf{b}$  field. There is no parity for modes in the T1S1 background field. The asterisk signifies  $\Lambda = 10$ .

mode	$m$	parity	$\tilde{\omega}$	$E_k/E_m$	characteristic	figure
M-E1	3	QP	$-633.1 + 733.0i$	$7.16 \times 10^{-5}$	columnar	1
T1-E1	1	DP	$-19.3 + 0.149i$	$8.25 \times 10^{-9}$	QFD	3a
T1-E2	3	QP	$-742.8 + 684.1i$	$7.85 \times 10^{-5}$	columnar	3b
T1-E3	1	QP	$-8.26 - 3.55i$	$1.89 \times 10^{-7}$	moderately columnar	10a
T1-E4	0	DP	$-\pi^2$	$4.45 \times 10^{-8}$	QFD*	15a
S1-E1	1	DP	$-201.9 - 106.1i$	$1.20 \times 10^{-7}$	field controlled	16a
S1-E2	1	DP	$-287.9 - 115.2i$	$1.94 \times 10^{-7}$	field controlled	16b
S1-E3	1	DP	$-293.1 + 119.8i$	$2.36 \times 10^{-6}$	moderately columnar	8
S1-E4	1	DP	$-115.3 - 3.88i$	$2.91 \times 10^{-7}$	moderately columnar	10b
S1-E5	0	DP	$-78.4 + 23.1i$	$4.85 \times 10^{-8}$	columnar in $u_\phi$	15b
T1S1-E1	5	—	$-2134 + 2555i$	$3.28 \times 10^{-4}$	columnar	6

**Table 2.** Normal mode eigenvalues for the Malkus field.  $\tilde{\omega}_{\text{ideal}} = 0 + i\omega_{\text{ideal}}$  is the eigenvalue for the ideal case;  $\tilde{\omega}$  is the eigenvalue for the corresponding diffusive case. Computed at  $E_\eta = 10^{-9}$ ,  $\Lambda = 1$ .

$k_s$	1	2	3	4	5	6
	$m = 1$					
$\tilde{\omega}_{\text{ideal}}$	$0 + 13.3i$	$0 + 31.3i$	$0 + 57.3i$	$0 + 91.3i$	$0 + 133.3i$	$0 + 183.3i$
$\tilde{\omega}$	$-10.3 + 1.6i$	$-37.9 + 15.2i$	$-93.5 + 35.7i$	$-166.8 + 73.4i$	$-262.6 + 120.3i$	$-379.1 + 181.2i$
	$m = 3$					
$\tilde{\omega}_{\text{ideal}}$	$0 + 77.1i$	$0 + 155.6i$	$0 + 257.7i$	$0 + 383.8i$	$0 + 533.9i$	$0 + 707.9i$
$\tilde{\omega}$	$-43.3 + 4.5i$	$-112.5 + 94.9i$	$-205.6 + 204.2i$	$-323.3 + 346.4i$	$-465.8 + 522.6i$	$-633.1 + 733.0i$

## (b) Malkus configuration

Since the Malkus field gives an analytical solution to the canonical ideal problem, it allows us to compare the effect of magnetic diffusion on the normal modes' eigenvalues and structures. In the ideal case,  $\mathbf{u}$  and  $\mathbf{b}$  have identical structures, see (A 2), and correspond to one inertial mode. In this section, we consider the effects of diffusion in the Malkus field, under the application of an insulating condition at  $r = 1$ . Obviously, there has always been an inconsistency in the boundary conditions satisfied at  $r = 1$  by the imposed background and the perturbation, but we can solve this problem nevertheless. We illustrate the effects of diffusion by focusing on the branch of almost columnar modes, which in the ideal case corresponds to the branch of QG inertial modes [9]. We list in table 2 the eigenfrequency  $\omega_{\text{ideal}}$  of the ideal problem and  $\tilde{\omega}$  of the diffusive problem for  $m = 1, 3$ ,  $k_s = 1, \dots, 6$  in (2.10). The frequencies of the diffusive modes agree better with  $\omega_{\text{ideal}}$  of the ideal case for higher overtones. Damping of these modes is significant, while diffusion tends to dramatically reduce the frequency of the fundamental mode.

Figure 1 shows a comparison between the normal mode for the canonical ideal Malkus configuration (essentially an inertial mode) and the corresponding dissipative MC mode (labelled M-E1) with insulating boundary condition. This mode corresponds to the sixth QG inertial mode at  $m = 3$ , with  $\omega_i \approx -0.02564$ . In the ideal case, the eigenfrequency is  $\omega = 707.9$ ,  $\mathbf{u}$  and  $\mathbf{b}$  have

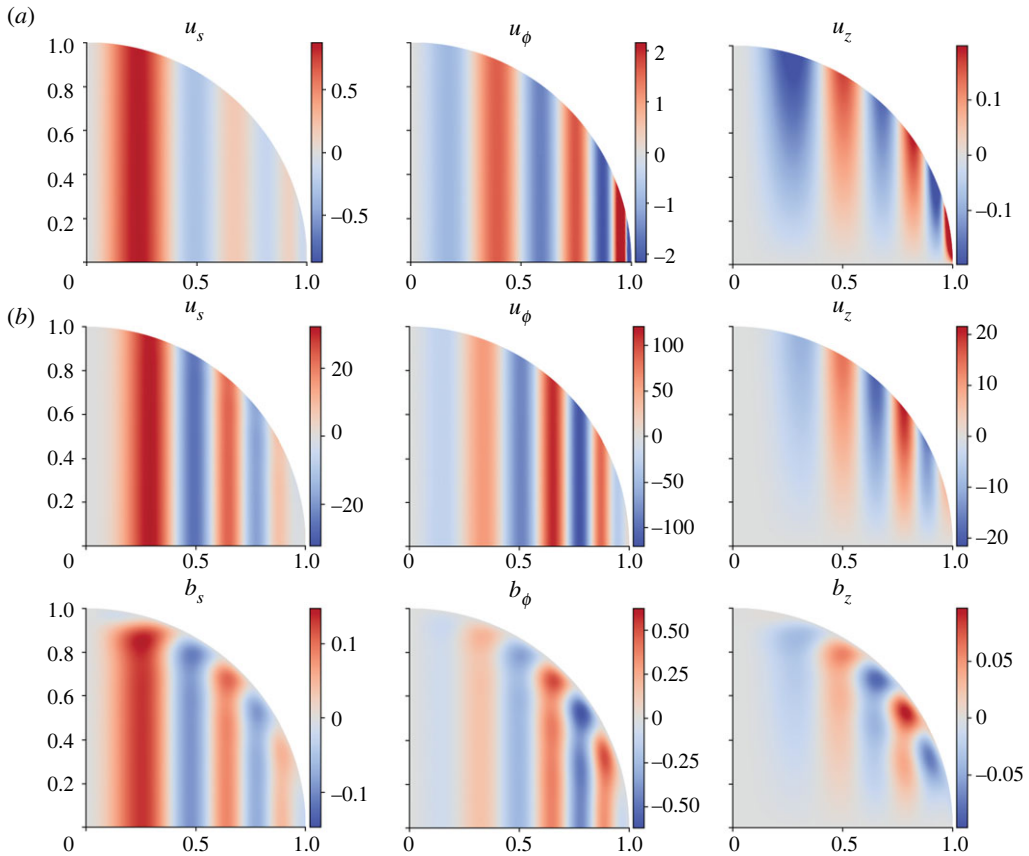


**Figure 1.** (a) The sixth quasi-geostrophic inertial mode with  $\omega_j = -0.02564$  at  $m = 3$ , correspondingly the ideal MC mode's frequency is  $\omega_{\text{ideal}} = 707.9$  in the Malkus configuration; (b) the corresponding dissipative MC mode with insulating boundary condition, labelled M-E1, is computed at  $E_\eta = 10^{-9}$  and  $\Lambda = 1$ . This mode has an eigenvalue  $\tilde{\omega} = -633.1 + 733.0i$ , with both  $u$  and  $b$  being **QP**. Field components are shown in cylindrical coordinates. Modes are computed at  $N = 60, L = 120$ . (Online version in colour.)

identical structures, thus only  $u$  is shown (first row of figure 1). The effect of dissipation on  $b$  is clearly seen in the last row of the plot, such that the columnar structure of  $b$  is modified with respect to the boundary condition. One minor effect seen for  $u$  is that its magnitude is actually much smaller at the equator due to the addition of dissipation and the insulating boundary condition, compared with the ideal case. This indicates that magnetic diffusion and the magnetic boundary condition might both play an important role for both the field and flow structures in the equatorial region if observed/inverted at the core-mantle-boundary, which the canonical ideal problem is unable to characterize. This mode can also be compared with the corresponding normal mode due the T1 toroidal background field in figure 3*b*. T1 consists of the same spherical harmonic as that of the Malkus field, but has a simple radial dependence that satisfies the insulating boundary condition, thus retains the consistency between  $B_0$  and  $b$ . Note that the Malkus field (2.8) does not satisfy the insulating boundary conditions.

### (c) T1 configuration

For the choice of a T1 background field, the perturbations  $u$  and  $b$  separate into independent symmetry groups such that they have the same equatorial parity. To illustrate the distribution of eigenvalues, we compute the whole eigen-spectrum at two resolutions,  $N = L = 30$  and 40. By

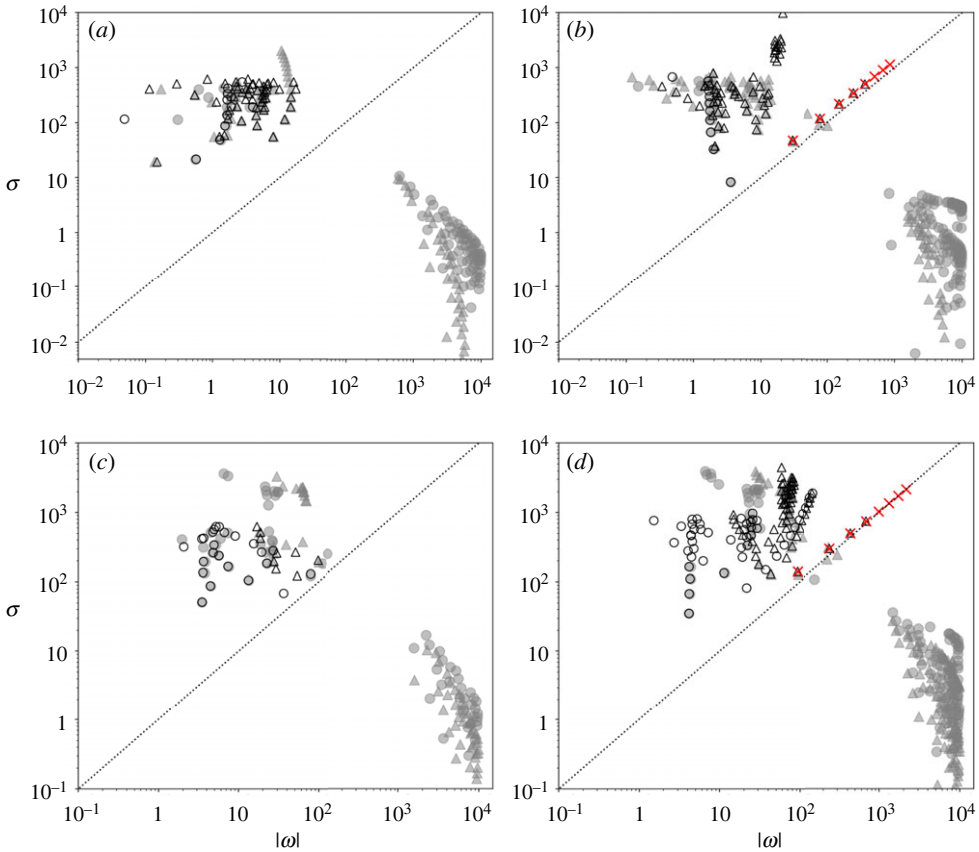


**Figure 2.** Selected resolved eigenvalues of the T1 configuration. The decay rate  $\sigma$  is plotted against the frequency  $|\omega|$  on a log-log scale. Eastward propagating modes are plotted with circles; westward propagating ones are plotted with triangles. Modes for  $E_\eta = 10^{-4}$  are plotted with solid grey symbols; modes for  $E_\eta = 0$  are plotted as empty black symbols. Computed at  $N = L = 40$ . The branch of westward propagating columnar MC modes listed in table 4 are plotted in red crosses, computed at  $E_\eta = 10^{-9}$ ,  $\Lambda = 1$ . (a)  $m = 1$ , **DP**; (b)  $m = 1$ , **QP**; (c)  $m = 3$ , **DP**; (d)  $m = 3$ , **QP**. (Online version in colour.)

comparing the eigenvalues at two different resolutions, we select the ones that are most likely to be converged via the eigenvalue drift method described in §7.5 of [41]. The selected ones are shown by their absolute frequency  $|\omega|$  and decay rate  $\sigma$  in figure 2 for  $m = 1$  and  $m = 3$ . For this case,  $E_\eta = 10^{-4}$  suffices to show good separation between the magnetic branch and inertial branch, shown with solid grey symbols. The inertial branch has a cutoff frequency at  $O(E_\eta^{-1}) = O(10^4)$ . For comparison, normal modes in the magnetostrophic limit  $E_\eta = 0$  have also been computed, shown as empty symbols, in which case only the magnetic branch is present. In the plot, eastward propagating modes ( $\omega < 0$ ) are shown with circles, while westward propagating modes ( $\omega > 0$ ) are plotted with triangles. For some simple MC modes, their independence on  $E_\eta$  as  $E_\eta \rightarrow 0$  (overlapping of solid and empty symbols) can readily be observed. We shall see in figures 4 and 5 that this trend becomes more obvious for background field S1 and T1S1 with  $E_\eta = 10^{-6}$ . All the MC modes are either over-damped ( $\sigma \gg |\omega|$ ) or critically damped ( $\sigma \sim |\omega|$ ). The least damped branch of modes are those slightly above the critical line of  $\sigma = |\omega|$  in the **QP** parity, which we shall see is a branch of modes with columnar  $\mathbf{u}$ . This would correspond to the slow branch to be found by any approximate theory using the columnar ansatz for  $\mathbf{u}$  [24,26,44–46]. Their frequencies and decay rates are consistent with the  $O(k^2)$  estimation we have made previously. Eigenvalues of this branch are listed in table 4 for  $E_\eta = 10^{-9}$  with higher spatial resolutions, and they are plotted

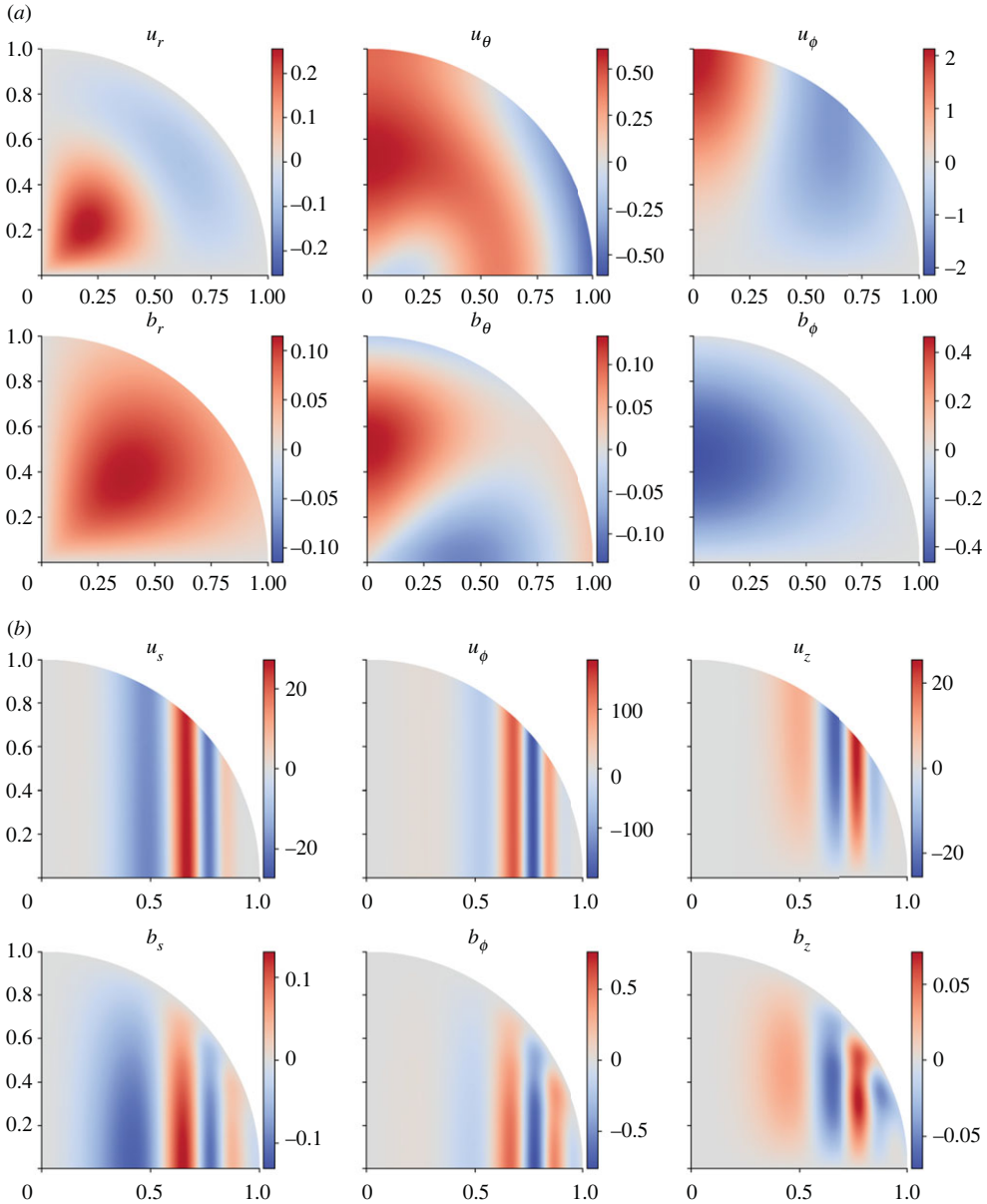


**Figure 3.** Normal modes in the T1 configuration. (a) T1-E1.  $m = 1$ ,  $\tilde{\omega} = -19.3 + 0.149i$ . Both  $\mathbf{u}$  and  $\mathbf{b}$  are of DP parity. (b) T1-E2.  $m = 3$ ,  $\tilde{\omega} = -742.8 + 684.1i$ . Both  $\mathbf{u}$  and  $\mathbf{b}$  are of QP parity. Field components of T1-E2 are shown in cylindrical coordinates. Both modes are computed at  $N = 60, L = 120$ , with  $E_\eta = 10^{-9}$  and  $\Lambda = 1$ . (Online version in colour.)

as red crosses in figure 2. It is worth remarking that for T1 most of the magnetic modes at  $m = 1$  are westward propagating with but a few exceptions; by contrast,  $m = 3$  has roughly east/west equipartition. This has also been observed with the Malkus background field (2.8), but is not seen for S1 or T1S1.

Figure 3*a,b* shows two normal modes at  $m = 1$  and  $m = 3$  with opposite equatorial parities. The mode labelled T1-E1 shown in figure 3*a*, with  $\tilde{\omega} = -19.3 + 0.149i$ , is found to be a QFD mode previously studied by [32]. The corresponding free decay mode is the slowest decaying toroidal field at  $m = l = 1$  with an analytical decay rate of  $\sigma = 20.19$ , comparable with  $\sigma = 19.3$  for T1-E1.

**Table 3.** Eigenvalues of the  $m = 3$  modes T1-E2 (figure 3b) and  $m = 1$  mode S1-E2 (figure 16b) with increasing resolution. The radial resolution is fixed to  $N = L/2$ ,  $E_\eta = 10^{-9}$  and  $\Lambda = 1$ . Note the westward (eastward) propagation direction for T1 (S1). The resolved digits are in bold.

L	T1-E2	S1-E2
40	$-740.1384100 + 677.4217904i$	$-287.9429392 - 115.2082312i$
60	$-742.8497293 + 684.05114i$	$-287.9444544 - 115.2084350i$
80	$-742.7665150 + 684.1328102i$	$-287.944767 - 115.2082567i$
100	$-742.7652159 + 684.1321693i$	$-287.94483298 - 115.2081568i$
120	$-742.7652176 + 684.132152i$	$-287.9448432 - 115.2081087i$

The difference between T1-E1 and the free decay mode is only 6% in terms of the magnetic energy. It is interesting to note that this mode is found outside the validity region  $\Lambda \ll 1$  according to [32]. The mode labelled T1-E2 shown in figure 3b with  $\tilde{\omega} = -742.8 + 684.1i$  is a columnar mode, for both  $u$  and  $b$ . Convergence of its eigenvalue is verified in table 3 for increasing numerical resolutions. We remark that MC modes for the Malkus field and T1 field (with only a difference in the radial function) are quite similar in a general and qualitative sense. This similarity is largely seen for the T1-E2 mode:  $u$  and  $b$  have nearly identical structures in the bulk and are in phase with each other. This is consistent with the diffusionless analytical result for the Malkus field, see (A2); note that  $\omega > 0$ , so that it propagates westwards. The mode is essentially critically damped ( $|\sigma| \approx \omega$ ). Despite the overall similarity, differences clearly present in their normal mode structures and eigenvalues, for example by comparing figures 1 and 3b.

#### (d) S1 configuration

For the choice of S1 background field, the perturbations  $u$  and  $b$  separate into independent symmetry groups such that they have opposite equatorial parities. We compute all eigenvalues at two resolutions,  $N = L = 30$  and 40, and selected ones (according to our criterion of §4c) are shown in figure 4. Due to a smaller  $E_\eta = 10^{-6}$ , the overlap between the MC modes at  $E_\eta = 10^{-6}$  and those in the magnetostrophic limit of  $E_\eta = 0$  is clearer compared with figure 2. Both eastward and westward propagating modes are found. However, in contrast to T1 (figure 2b,d) and T1S1 (figure 5), there does not exist an obvious branch of westward propagating MC modes with columnar  $u$ . Some columnar modes exist, but with only moderate columnarity, see §5a. Nevertheless, there exists branches of modes propagating along with the dipolar field lines and also transverse to them. S1-E1 and S1-E2 shown in appendix B are two examples of them. We refer to these modes as being field controlled, and discuss them in some detail in appendix B. The eigenvalue of S1-E2 is also verified in table 3.

#### (e) T1S1 configuration

For background field T1S1, normal modes have a mixture of both DP and QP parities. Figure 5 shows the eigenvalue distribution computed from low resolutions for  $m = 1$  and  $m = 5$  at  $E_\eta = 10^{-6}$ . By adding the toroidal component T1 to S1, we are able to find again the distinguished branch of columnar modes. Eigenvalues for  $E_\eta = 10^{-9}$  are generally not shown, with the exception that those listed in table 4 (of columnar modes) are plotted with red crosses; these eigenvalues overlap almost perfectly with the  $E_\eta = 0$  calculations (empty black triangles), while eigenvalues at  $E_\eta = 10^{-6}$  (solid grey triangles) do not for higher overtones. These modes are located near the critical line of  $\sigma = |\omega|$ , and are all westward propagating. Figure 6 shows an example of such a mode at  $m = 5$ . Breaking of the equatorial parity is seen for  $u_z$  and all components of  $b$ , and the azimuthal component dominates both fields. One can also observe the effects of magnetic diffusion, forming little patches at both ends of the distorted columnar structure of  $b$ . As  $B_0$

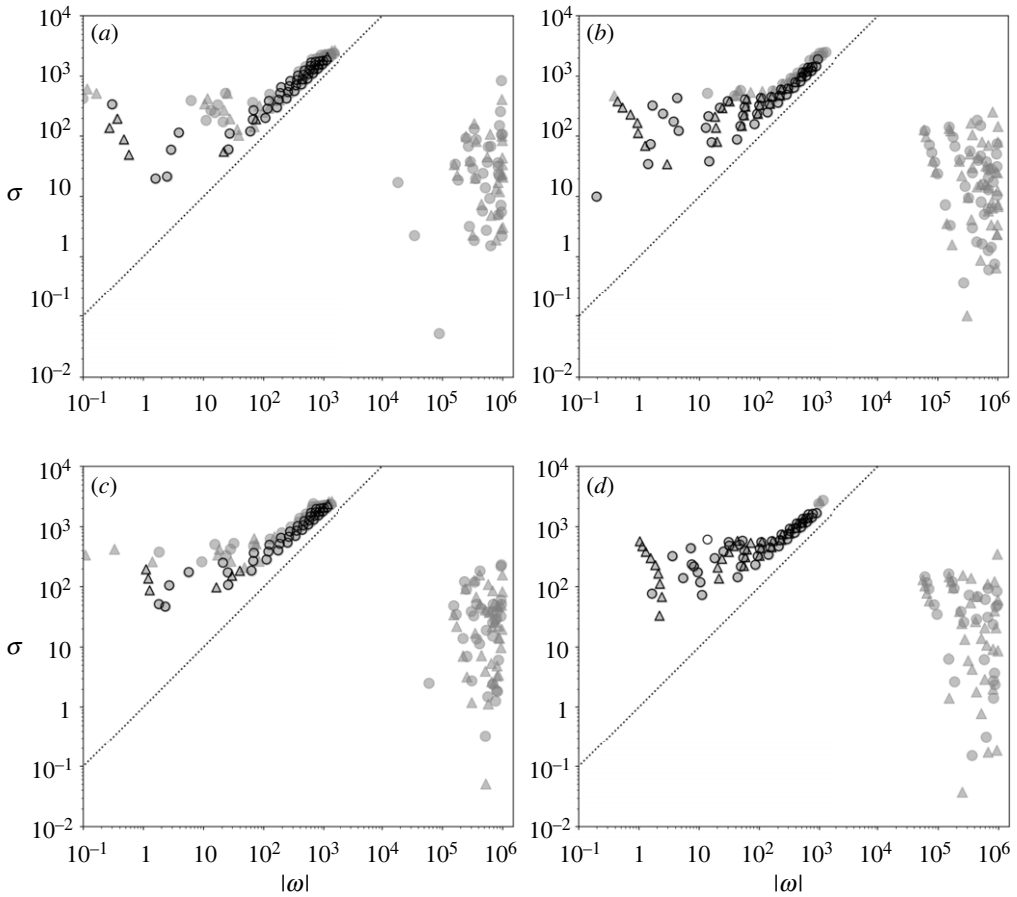


**Figure 4.** Selected eigenvalues of S1 configuration. The decay rate  $\sigma$  is plotted against the frequency  $|\omega|$  on a log-log scale. Eastward propagating ones are plotted with circles; westward propagating ones are plotted with triangles. Modes for  $E_\eta = 10^{-6}$  are plotted with solid grey symbols; modes for  $E_\eta = 0$  are plotted as empty black symbols. Computed at  $N = L = 40$ . (a)  $m = 1$ , DP; (b)  $m = 1$ , QP; (c)  $m = 3$ , DP; (d)  $m = 3$ , QP.

**Table 4.** Eigenvalues of the branch of columnar modes in the T1 and T1S1 configurations.  $k_s$  is an integer assigned to describe the complexity in  $s$ . Propagation is westwards in all cases.

$k_s$	T1, $m = 1$	T1, $m = 3$	T1S1, $m = 1$	T1S1, $m = 5$
3	$-47.7 + 29.6i$	$-140.3 + 93.6i$	$-44.8 + 11.3i$	$-195.0 + 83.6i$
4	$-118.6 + 78.6i$	$-298.4 + 239.7i$	$-103.7 + 37.7i$	$-369.8 + 228.9i$
5	$-217.8 + 150.8i$	$-499.1 + 437.3i$	$-178.6 + 82.6i$	$-586.9 + 427.1i$
6	$-345.7 + 245.4i$	$-742.8 + 684.1i$	$-294.4 + 185.8i$	$-846.0 + 685.6i$
7	$-502.1 + 362.6i$	$-1029.8 + 979.2i$	$-454.7 + 364.5i$	$-1142.4 + 1005.7i$
8	$-686.9 + 502.2i$	$-1360.2 + 1322.3i$	$-664.6 + 639.3i$	$-1455.2 + 1399.3i$
9	$-900.2 + 664.3i$	$-1734.1 + 1713.0i$	$-927.8 + 1034.6i$	$-1777.6 + 1907.7i$
10	$-1141.7 + 849.0i$	$-2151.3 + 2151.4i$	$-1250.9 + 1579.4i$	$-2134.0 + 2555.2i$

becomes more complicated, it is not straightforward to classify modes into clear branches as was done for S1. Nevertheless, we have seen some modes that are very similar to, for example, figure 16a.

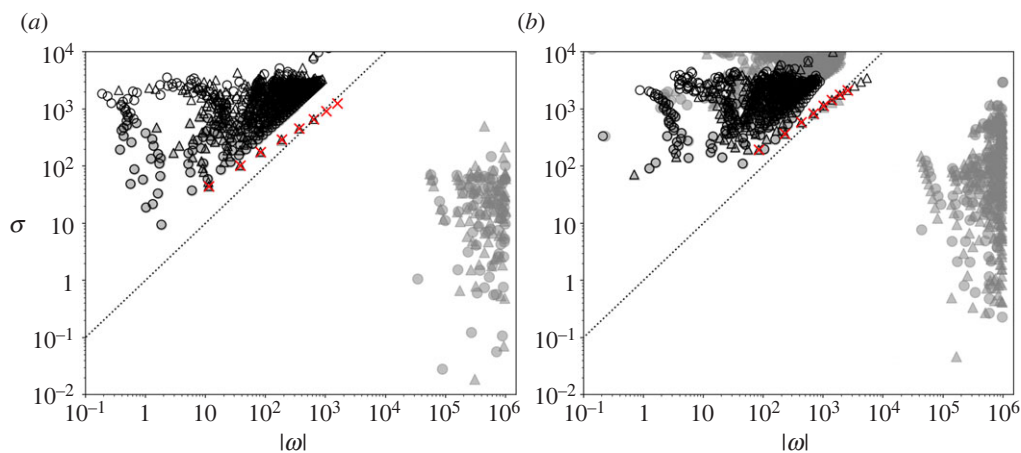


**Figure 5.** Selected eigenvalues of the T1S1 configuration. The decay rate  $\sigma$  is plotted against the frequency  $|\omega|$  on a log-log scale. Eastward propagating ones are plotted with circles; westward propagating ones are plotted with triangles. Modes for  $E_\eta = 10^{-6}$  are plotted with solid grey symbols; modes for  $E_\eta = 0$  are plotted as empty black symbols.  $E_\eta = 10^{-6}$  cases are computed at  $N = L = 40$ ,  $E_\eta = 0$  cases are computed at  $N = 40, L = 80$ . The branch of westward propagating columnar MC modes listed in table 4 are plotted as red crosses, computed at  $E_\eta = 10^{-9}$ ,  $\Lambda = 1$ . (a)  $m = 1$ ; (b)  $m = 5$ . (Online version in colour.)

## 5. Discussion

### (a) Columnar magneto–Coriolis modes

We have remarked in §4 that, for T1 and T1S1, there exists a branch of columnar modes, with two examples of them given in figures 3*b* and 6. We identify normal modes from this branch for  $E_\eta = 10^{-9}$ ,  $\Lambda = 1$  and their eigenvalues are summarized in table 4. Eigenvalues of these modes are also marked as red crosses in figures 2 and 5. It is desirable to assign a single wavenumber  $k_s$  in the cylindrical radial direction to each of these modes. However, in contrast to the ideal case, magnetic diffusion renders the eigenvalue complex together with complex eigenmodes. Assigning a single  $k_s$  is not straightforward. As the system is linear, arbitrary phase factors can multiply an eigenmode, resulting in different views of the eigenmode. For example, consider the first mode of the T1,  $m = 1$  case listed in table 4. Depending on the choice of the arbitrary phase factor, the real part of the cylindrical average of  $u_\phi$ , as a function of  $s$ , can have three or four roots for  $s \in [0, 1]$ . We choose to begin the count at  $k_s = 3$  and every subsequent mode increases  $k_s$  by one. Wavenumbers  $k_s$  for the other three cases listed in table 4 are assigned in the same way. We find that columnar modes that should correspond to  $k_s = 1$  or 2 (fewer roots, larger length scale) do not exist along the same branch, which can largely be seen from figures 2*b,d* and 5. The columnarity or westward propagation property of  $k_s = 1$  and 2 modes may be lost because the modes are too simple or are mixed with other non-columnar modes. Magnetic dissipation may also contribute to shifting the eigenvalue and changing the structure of simple normal modes. This phenomenon could possibly be linked with the dramatic reduction of frequency of the fundamental columnar MC mode in table 2 of the Malkus field by introducing the magnetic diffusion. We plot in figure 7, the frequencies and decay rates of the columnar modes listed in table 4. For T1 (solid lines), values of  $\omega/m$  nearly collapse for  $m = 1$  and  $m = 3$  with a scaling of  $k_s^2$ . By combining (2.9) and (2.10), one sees that this is consistent with the analytical diffusionless result of the Malkus field, providing more evidence of the similarity between the T1 and Malkus cases. For T1S1, the scalings for  $m = 1$  and  $m = 5$  are very different, and the  $m = 1$  eigenfrequency has a clearly steeper scaling than  $k_s^2$ , indicating a different mechanism for the mode compared with the simple T1 case.

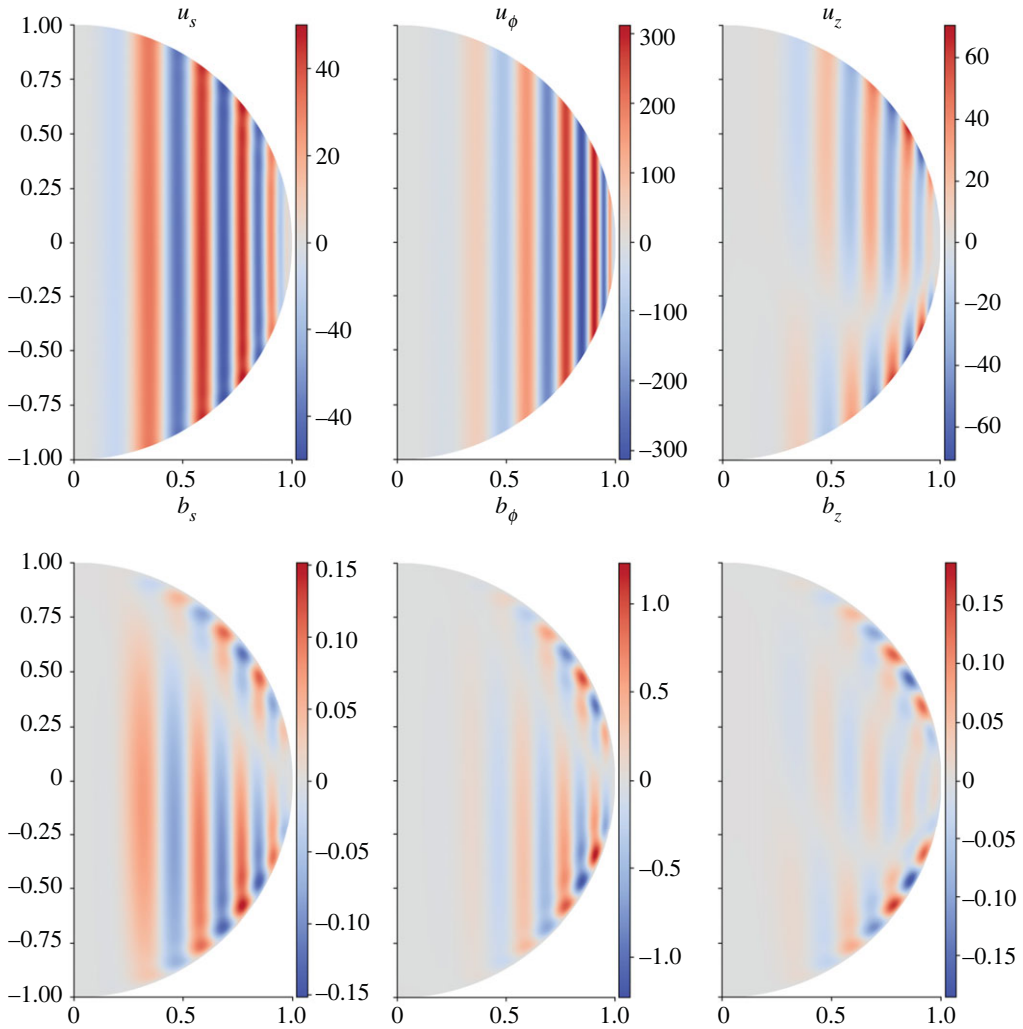


**Figure 6.** Normal mode T1S1-E1. T1S1 configuration,  $m = 5$ ,  $\tilde{\omega} = -2134 + 2555i$ . It is computed at  $L = 2N = 120$ , with  $E_\eta = 10^{-9}$  and  $\Lambda = 1$ . Field components in cylindrical coordinates are shown. (Online version in colour.)

For S1, we are not able to find such a branch of nearly perfect columnar modes. Some exist, but do not form a branch such that modes continue to exist for higher wavenumbers. Empirically, this seems to be related to the lack of a  $B_\phi$  component in the background field. In order to measure how columnar a flow  $u$  is, we define a quantity  $\chi(s)$ , termed *columnarity*, as

$$\chi(s) = \sqrt{\frac{|\{u_s\}|^2 + |\{u_\phi\}|^2}{\{|u_s|^2 + |u_\phi|^2\}}}(s), \quad (5.1)$$

in which complex functions  $u_s = u_s(s, z)$  and  $u_\phi = u_\phi(s, z)$  are the cylindrical components of  $u$  without the azimuthal dependence  $e^{im\phi}$ .  $\{\}$  is the cylindrical average operator we have defined previously.

Besides the branch of columnar modes, there exist other normal modes with slightly weaker columnarity. Figure 8 shows such an example for S1 configuration with  $\tilde{\omega} = -293.1 + 119.8i$  (labelled as S1-E3). It is obvious from the plot that both  $u_\phi$  and  $u_s$  are less columnar compared

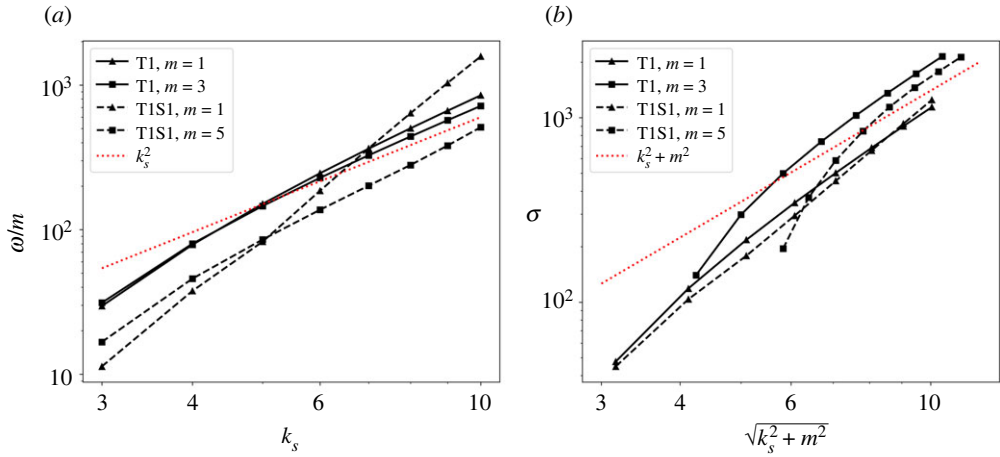


**Figure 7.** For the columnar modes of table 4: (a) eigenfrequency  $\omega/m$  plotted against  $k_s$ ; (b) decay rate  $\sigma$  plotted against  $\sqrt{k_s^2 + m^2}$ . T1 symmetry is solid, mixed symmetry T1S1 is dashed. (Online version in colour.)

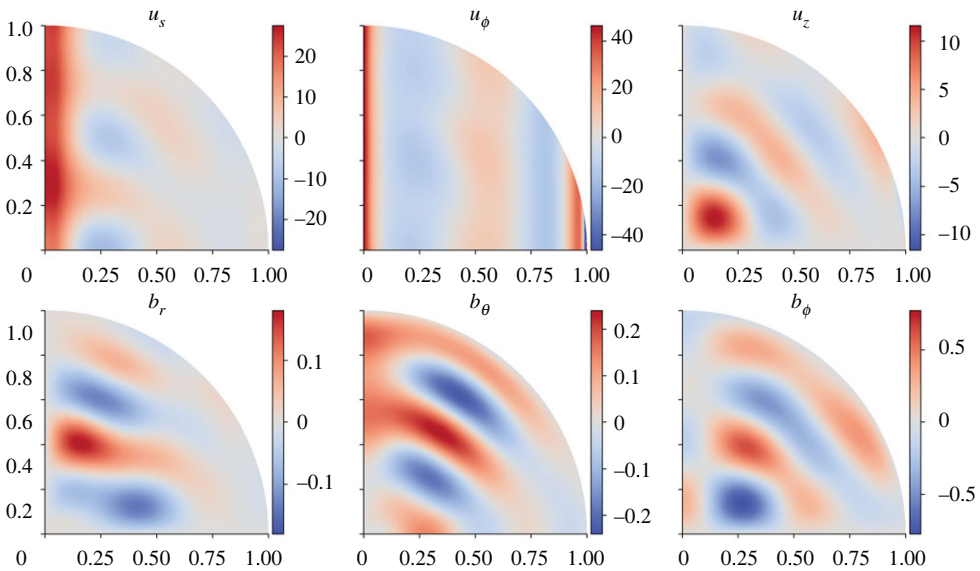


**Figure 8.** Normal mode S1-E3. S1 configuration,  $m = 1$ ,  $\tilde{\omega} = -293.1 + 119.8i$ .  $\mathbf{u}$  is **QP** and  $\mathbf{b}$  is **DP**. It is computed at  $E_\eta = 10^{-9}$ ,  $\Delta = 1$ ,  $L = 2N = 120$ . (Online version in colour.)

with those in figure 3b and figure 6. Figure 9 plots  $\chi(s)$  of the moderately columnar mode S1-E3 (blue line). As a comparison,  $\chi(s)$  for the columnar modes in table 4 with  $m = 1$  are plotted with black dashed lines. The difference in columnarity is clearly seen. For convenience, in terms of terminology, we shall refer to a mode being columnar if  $\chi(s) \geq 0.95$  for all  $s$ , and shall use the term moderately columnar for modes with  $\chi(s)$  generally larger than 0.9 possibly with an exception in a small range of  $s$ , such as S1-E3. We find these moderately columnar MC modes to exist generally for different  $B_0$ , but it is hard to see them as a clear branch of modes. Moreover, compared with modes in the columnar branch, these moderately columnar ones generally have a larger

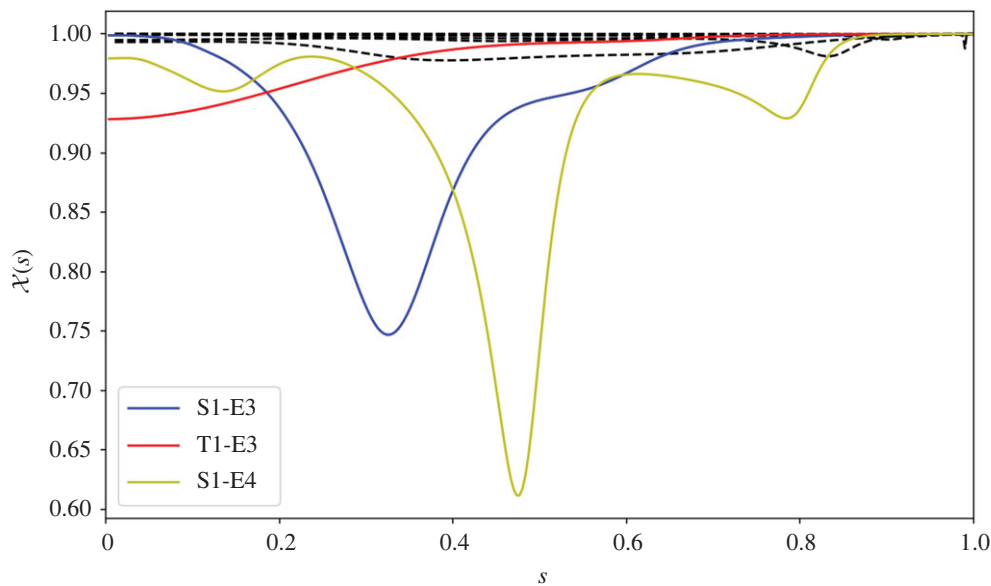


**Figure 9.**  $\chi(s)$  for S1-E3 of figure 8 (blue), T1-E3 of figure 10a (red) and S1-E4 of figure 10b (yellow).  $\chi(s)$  for  $m = 1$  columnar modes in table 4 are plotted as black dashed lines for comparison. (Online version in colour.)

ratio of  $|\sigma|/|\omega|$ . Consequently, they are of less geophysical interest compared with the columnar branch.

### (b) Propagation direction of columnar magneto–Coriolis modes

With the columnar ansatz for  $\mathbf{u}$ , the result of [24] has been reproduced in many works, namely that the slow MC branch propagates westward and the fast inertial branch propagates eastward [26,27]. This also holds true for the diffusionless three-dimensional case with a Malkus background field. This can be verified by substituting (2.10) into (2.9). However, no proof exists that excludes the existence of eastward propagating MC modes with columnar  $\mathbf{u}$  for the three-dimensional case with magnetic diffusion and a general  $\mathbf{B}_0$ . In fact, [32] has shown in a sphere (technically a spherical shell with an inner core of radius 0.35) that eastward propagating columnar MC modes can exist in the form of quasi-free decay modes, in the regime of  $\Lambda \ll 1$ . However, the nature of such modes is that of almost pure decay, thus it is questionable if these modes generally exist for  $\Lambda \geq O(1)$ . For  $\Lambda = 1$ , we are able to find some eastward propagating MC modes with (moderately) columnar  $\mathbf{u}$  for all three configurations of  $\mathbf{B}_0$ . Figure 10a,b shows two such examples for T1 and S1, labelled as T1-E3 and S1-E4, respectively. It is interesting to remark that the T1-E3 mode in figure 10a is significant in that it happens to have the smallest absolute decay rate in figure 2b. One may regard this mode as a continuation of the branch of westward propagating columnar modes marked by red crosses. The columnarity  $\chi(s)$  of T1-E3 and S1-E4 are plotted as the red and yellow lines, respectively, in figure 9. Compared with the westward propagating columnar modes of table 4, the eastward propagating ones are generally less columnar, which is seen from figure 9. We found these modes to exist regardless of the choice of background magnetic field. Frequencies of these eastward propagating columnar modes, being mostly at  $O(1)$ , are often small in comparison with their decay rates. Thus the existence of this type of mode relies heavily on the effect of the magnetic diffusion. Eastward propagating structures have been observed in the numerical simulations of [28]. It remains to be seen if there is any correspondence between their observation and the modes presented here. The phase speeds of the modes found here are too small to account for the observations in their numerical simulation.

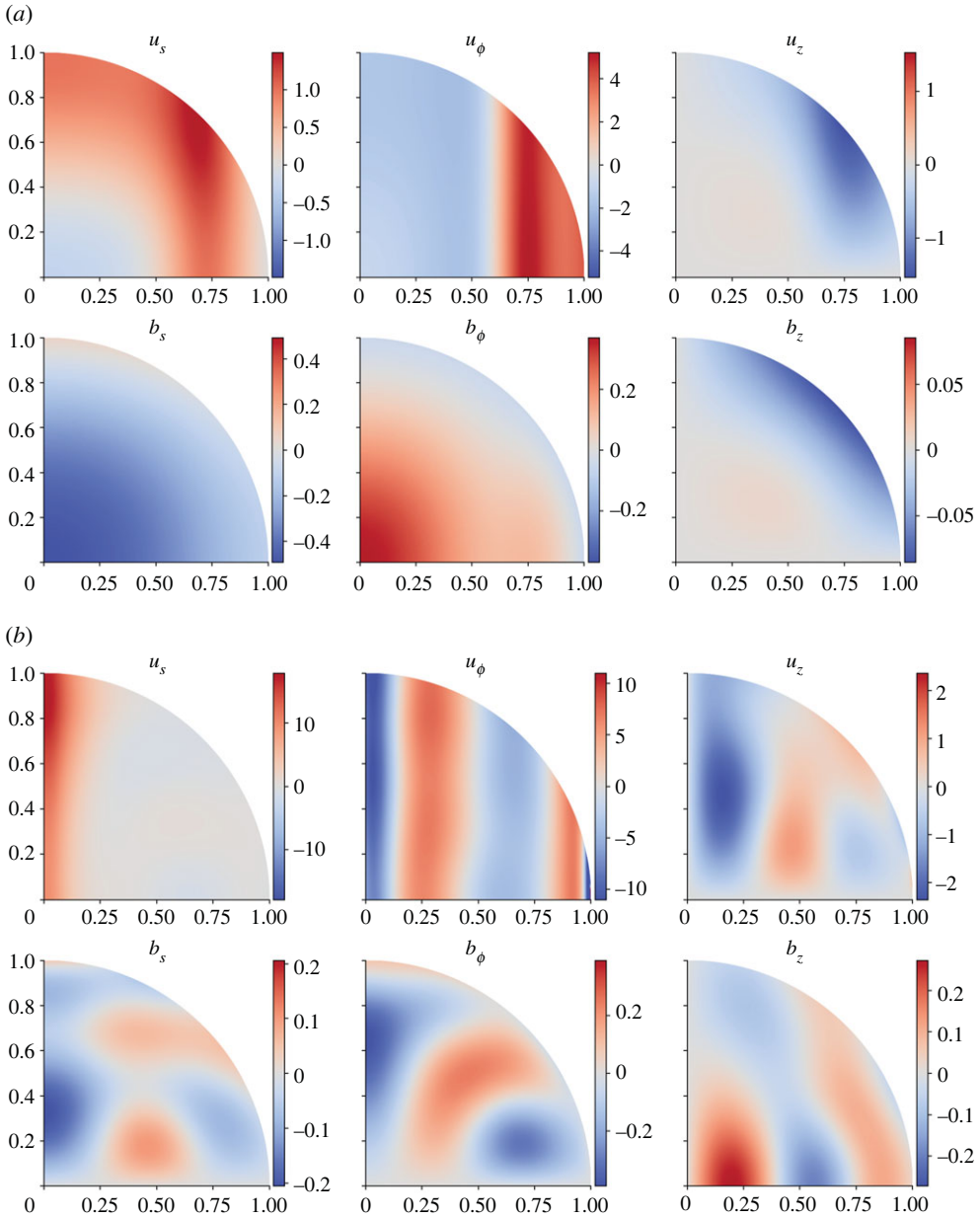


**Figure 10.** Two examples of eastward propagating MC modes for T1 and S1 configurations. Field components are shown in cylindrical coordinates. (a) Eastward propagating normal mode T1-E3. T1 configuration,  $m = 1$ ,  $\tilde{\omega} = -8.26 - 3.55i$ . Both  $\mathbf{u}$  and  $\mathbf{b}$  are QP. (b) Eastward propagating normal mode S1-E4. S1 configuration,  $m = 1$ ,  $\tilde{\omega} = -115.3 - 3.88i$ .  $\mathbf{u}$  is QP and  $\mathbf{b}$  is DP. Both modes are computed at  $E_\eta = 10^{-9}$ ,  $\Lambda = 1$ ,  $L = 2N = 120$ . (Online version in colour.)

### (c) The magnetostrophic limit

As largely seen in the eigenvalue plots figures 2, 4 and 5, by taking  $E_\eta \rightarrow 0$ , eigenvalues of the MC modes tend to closely agree with the eigenvalue obtained in the singular limit of  $E_\eta = 0$ . To illustrate the dependence on  $E_\eta$ , we take the mode T1-E2 shown in figure 3b as an example, and compute its eigenvalue as a function of  $E_\eta$ , shown in figure 11. The frequency  $\omega$  converges to its asymptotic value faster than does the decay rate  $\sigma$ . For modes with large or moderate spatial scales, the Earth-like value of  $E_\eta = 10^{-9}$  is certainly in the asymptotic regime of magnetostrophy.

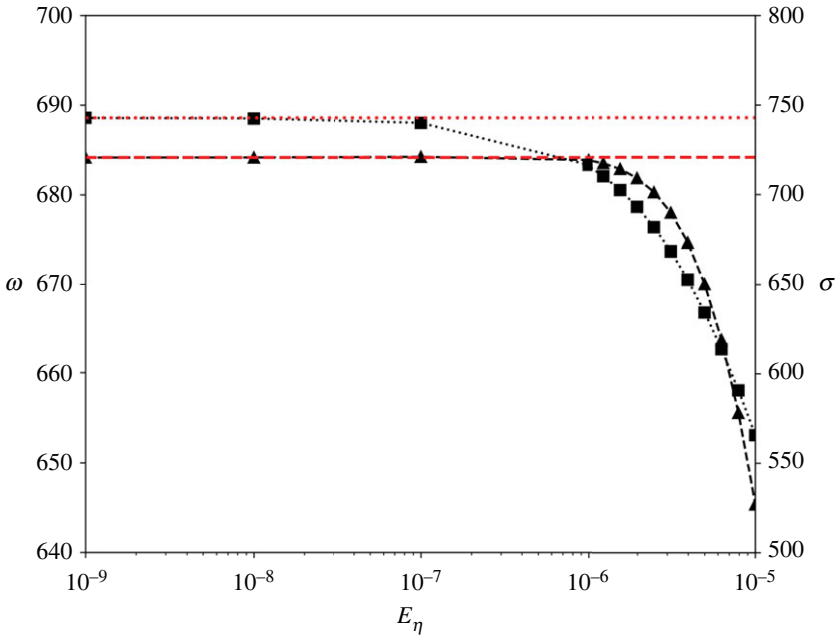


**Figure 11.** Frequency  $\omega$  (triangles, black dashed line) and decay rate  $\sigma$  (squares, black dotted line) as a function of  $E_\eta$  for mode T1-E2 shown in figure 3*b*. The asymptotic case of  $E_\eta = 0$  is shown in the red dashed line and dotted line for  $\omega$  and  $\sigma$ , respectively. (Online version in colour.)

### (d) Energy partitioning

In table 1, we have listed the ratio between kinetic and magnetic energies (as defined in equation (A 8)) for modes presented herein. These are all computed at  $E_\eta = 10^{-9}$  and  $\Lambda = 1$ , except for mode T1-E4 being at  $\Lambda = 10$ . For the plane wave solution in an infinite space discussed in the Introduction, the ratio between kinetic and magnetic energy is given by

$$\frac{E_k}{E_m} = \left| \frac{\omega_M}{\omega_C^2} \right|. \quad (5.2)$$

This is qualitatively consistent with those listed in table 1. Modes of more complex structures (larger  $k$ ) or with columnar  $\mathbf{u}$  (smaller  $\omega_C$ ) tend to have a larger proportion of kinetic energy. Among them, the most small-scale columnar mode T1S1-E1 has the highest  $E_k/E_m$ , but is still only at the order of  $O(10^{-4})$ . Our calculation shows that, as expected, MC modes of moderate complexity have dominant magnetic energy at Earth-like parameters.

### (e) Dependence on $\Lambda$

The Elsasser number  $\Lambda$  for the Earth is estimated to be  $O(1) \sim O(10)$ . In this section, we investigate the MC modes' dependence on the Elsasser number. Figure 12 shows the frequency and decay rate of two of the simplest modes ( $k_s = 3$ ) of table 4, namely of T1,  $m = 3$  and T1S1,  $m = 5$  for  $\Lambda \in [0.1, 10]$ . Both  $\omega$  and  $\sigma$  increase with  $\Lambda$ . The diffusionless analytical result (A 7) for the Malkus field shows that  $\omega$  has a linear dependence on  $\Lambda$ . However, figure 12 indicates that  $\omega$ 's dependence on  $\Lambda$  for a more realistic set-up is sublinear in  $\Lambda$ . As  $\Lambda$  is increased, the normal mode structure also changes. Figure 13 shows the components of  $\mathbf{u}$  for  $\Lambda = 1, 10$  of the two modes considered. A stronger Lorentz force as a result of larger  $\Lambda$  renders the effect of rotation weaker, thus the columnar structure of  $\mathbf{u}$  is gradually lost as  $\Lambda$  increases. However, the columnar structure of  $\mathbf{u}$  remains localized to the equatorial region, which is likely to be due to the fact that  $\mathbf{B}_0$  is weak at the equator.

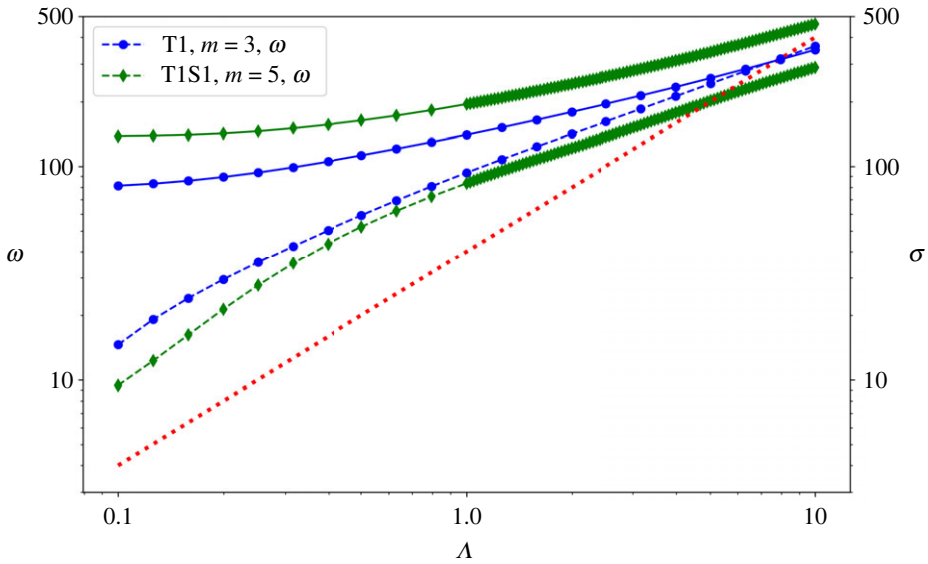


**Figure 12.** Elsasser number  $\Delta$  dependence of the  $k_s = 3$  mode in table 4 for T1,  $m = 3$  (blue circles) and T1S1,  $m = 5$  (green diamonds). Frequencies  $\omega$  (dashed lines) are shown on the left axis, and decay rates (solid lines) are shown on the right axis. The red dotted line shows a scaling proportional to  $\Delta$  for comparison. More eigenmodes for the T1S1 case are evaluated to avoid jumping into other eigenmodes while varying  $\Delta$ . (Online version in colour.)

### (f) Dissipation of MC modes

For diffusive TOs in an axisymmetric background field, it has been seen that the magnetic dissipation either occurs near the axis or at the equatorial region [30], depending on the Alfvén velocity profile and the normal mode's frequency  $\omega$ . We plot  $|\nabla \times \mathbf{b}|$  for two examples of columnar MC modes from T1 and T1S1 in figure 14. The T1 example exhibits mainly internal dissipation, while dissipation for the T1S1 example is mainly located at the middle latitude spherical boundary. This is largely seen in figure 6 for a similar mode of T1S1 at  $k_s = 10$ , where little structures in  $\mathbf{b}$ 's components are formed in order to satisfy the insulating boundary condition. The strongest dissipation is within the magnetic boundary layer. Canet *et al.* [26] have reported the comparison between the oscillation period  $T_{\text{MC}} = 2\pi/|\omega|$  and decay time  $T_{\text{decay}} = 2\pi/\sigma$ . They have found for  $\Delta = 5$  (using our  $\Delta$  definition of equation (2.5)) that the Malkus field gives  $T_{\text{MC}} < T_{\text{decay}}$ , while a general background field gives  $T_{\text{MC}} > T_{\text{decay}}$ . This is not seen for our analogy T1 of the Malkus field: at  $\Delta = 10$ ,  $T_{\text{MC}} \approx T_{\text{decay}}$ . This is probably due to their use of a two-dimensional potential formulation of the magnetic field. We remark that the magnetic field  $\mathbf{b}$  corresponding to  $\mathbf{u}$  in figure 13 is not columnar, thus the  $z$ -invariant  $A$ -formulation for  $\mathbf{b}$  (as used by [26]) is not valid, and additional diffusion needs to be taken into account due to  $z$ -derivatives of  $\mathbf{b}$ . For our more general background field T1S1,  $T_{\text{decay}}$  is slightly shorter than  $T_{\text{MC}}$  for the fundamental ( $k_s = 3$ ) mode, but table 4 shows that  $T_{\text{MC}} < T_{\text{decay}}$  for higher overtones even at  $\Delta = 1$ .

### (g) Damping of fast modes

Although the focus of our study is the slow modes, we remark on the difference in damping rate of the fast modes between the two field configurations T1 and S1. Our modes are entirely damped magnetically and it is likely for modes containing large kinetic energy that it is the (omitted) viscous damping that is paramount for  $\Delta \ll 1$ , particularly if a non-slip condition were to be adopted (see [32]). However, we note from figures 2 and 4 that the decay rates from Ohmic

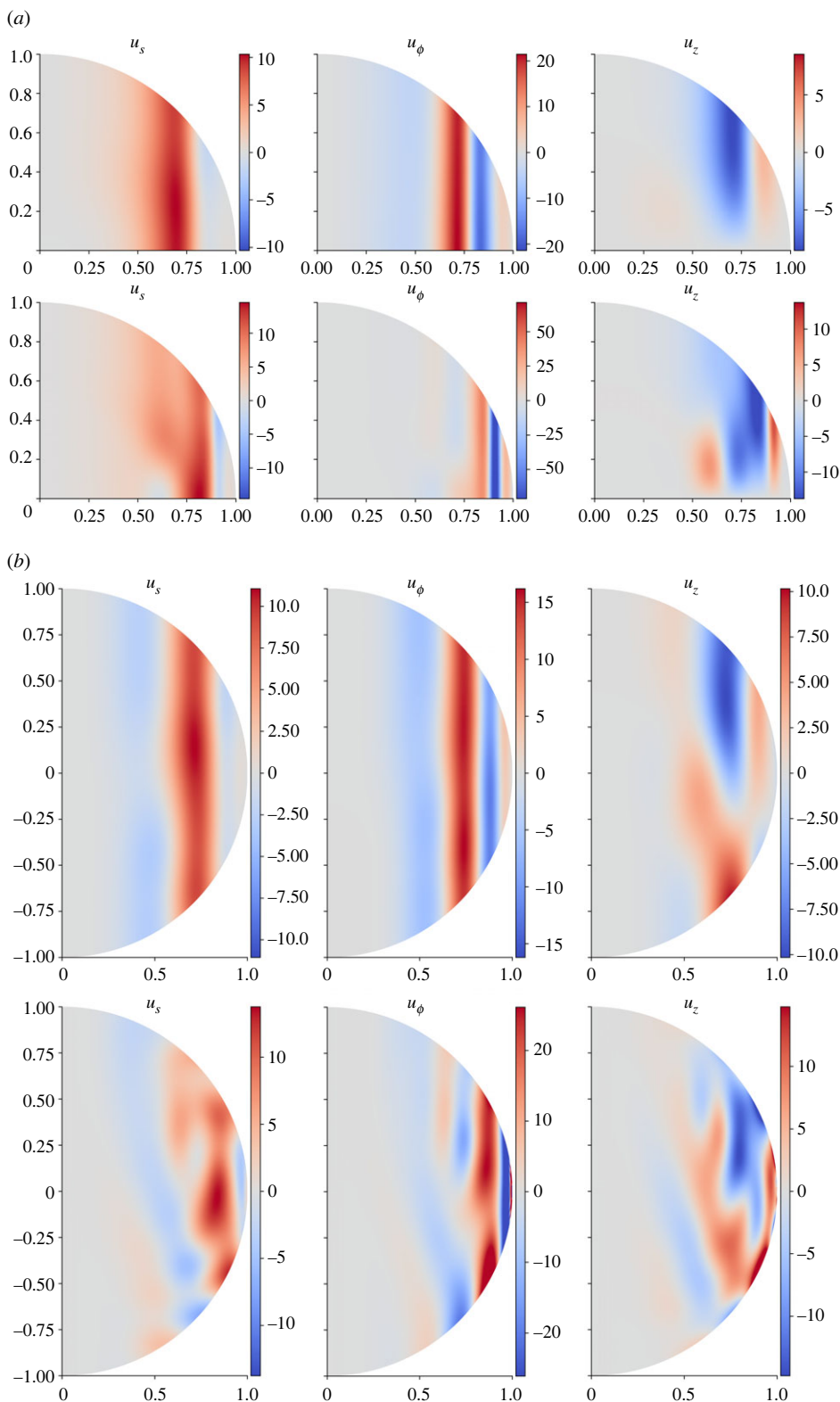


**Figure 13.** Comparison of T1 and T1S1 results at different Elsasser numbers. Field components of  $\mathbf{u}$  are shown in cylindrical coordinates. Modes are computed at  $2N = L = 220$ . (a) T1 configuration,  $m = 3$ ,  $k_s = 3$ ,  $\Lambda = 1$  (top row) and  $\Lambda = 10$  (bottom row). (b) T1S1 configuration,  $m = 5$ ,  $k_s = 3$ ,  $\Lambda = 1$  (top row) and  $\Lambda = 10$  (bottom row). (Online version in colour.)

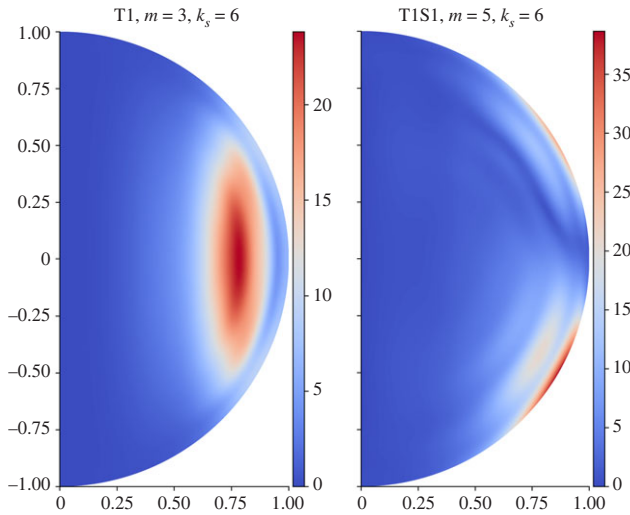


**Figure 14.**  $|\nabla \times \mathbf{b}|$  for two columnar MC modes from table 4. (a) T1,  $m = 3, k_s = 6$ , equatorial symmetric; (b) T1S1,  $m = 5, k_s = 6$ . Modes are computed at  $2N = L = 120$ . (Online version in colour.)

damping are generally larger for the S1 configuration than for T1, being almost 100 times larger for S1 compared with T1. These overall values are small compared with the modes' frequencies and the modes still have high quality factors.

The effect of the magnetic field on these modes has been the subject of several recent studies. Focusing on the spin-over node, [47] find that for  $\Lambda \geq 1$  and low  $Pm$ , Ohmic and viscous dissipation contribute nearly equally to the decay rate when the imposed field is uniform and the fluid is contained in a Earth-like shell with rigid boundary conditions. Working with stress-free boundary conditions in a spherical shell, [48] found that Ohmic dissipation was the predominant mechanism when  $P_m = 10^{-6}$  as in the Earth,  $\Lambda \geq 10^{-1}$  and the Ekman number  $E$  was  $10^{-9}$ . They demonstrated that the Ohmic dissipation, which can be more than three orders of magnitude greater than the viscous dissipation, becomes largely independent of  $\Lambda$ .

### (h) Axisymmetric magneto–Coriolis modes

Besides non-axisymmetric MC modes, we also find axisymmetric MC normal modes. We show two such examples for T1 and S1 in figure 15. The T1-E4 mode computed at  $\Lambda = 10$ , shown in figure 15a, has a purely real eigenvalue and its decay rate is identical to the least free-decay rate  $\pi^2$  of the magnetic field, up to numerical precision. However, the magnetic perturbation  $\mathbf{b}$  is not identical to the corresponding dipolar free-decay eigenmode with the same decay rate. The toroidal component constitutes about 20% of the total magnetic energy. Existence of such a purely decaying mode is likely to be due to the axisymmetric toroidal background field of T1, with which the induction term  $\nabla \times (\mathbf{u} \times \mathbf{B}_0)$  contributes only to changes of the toroidal magnetic field at  $m = 0$ . Consequently, poloidal  $\mathbf{b}$  is subject to pure decay. For the S1 configuration, magnetic induction contributes to both toroidal and poloidal components of  $\mathbf{b}$ , and thus the S1-E5 mode, shown in figure 15b, is of complex eigenvalue. In this example,  $\mathbf{b}$  is DP and  $\mathbf{u}$  is QP. An interesting aspect of this mode is that  $u_\phi$  is nearly geostrophic, while  $u_s$  is not. Components of  $\mathbf{b}$  are similar to the typical field controlled modes found in non-axisymmetry.

## 6. Summary and conclusion

Here, we summarize the most important conclusions, which we believe are amply substantiated by the foregoing calculations. Paramount to our calculations is the use of an extremely accurate

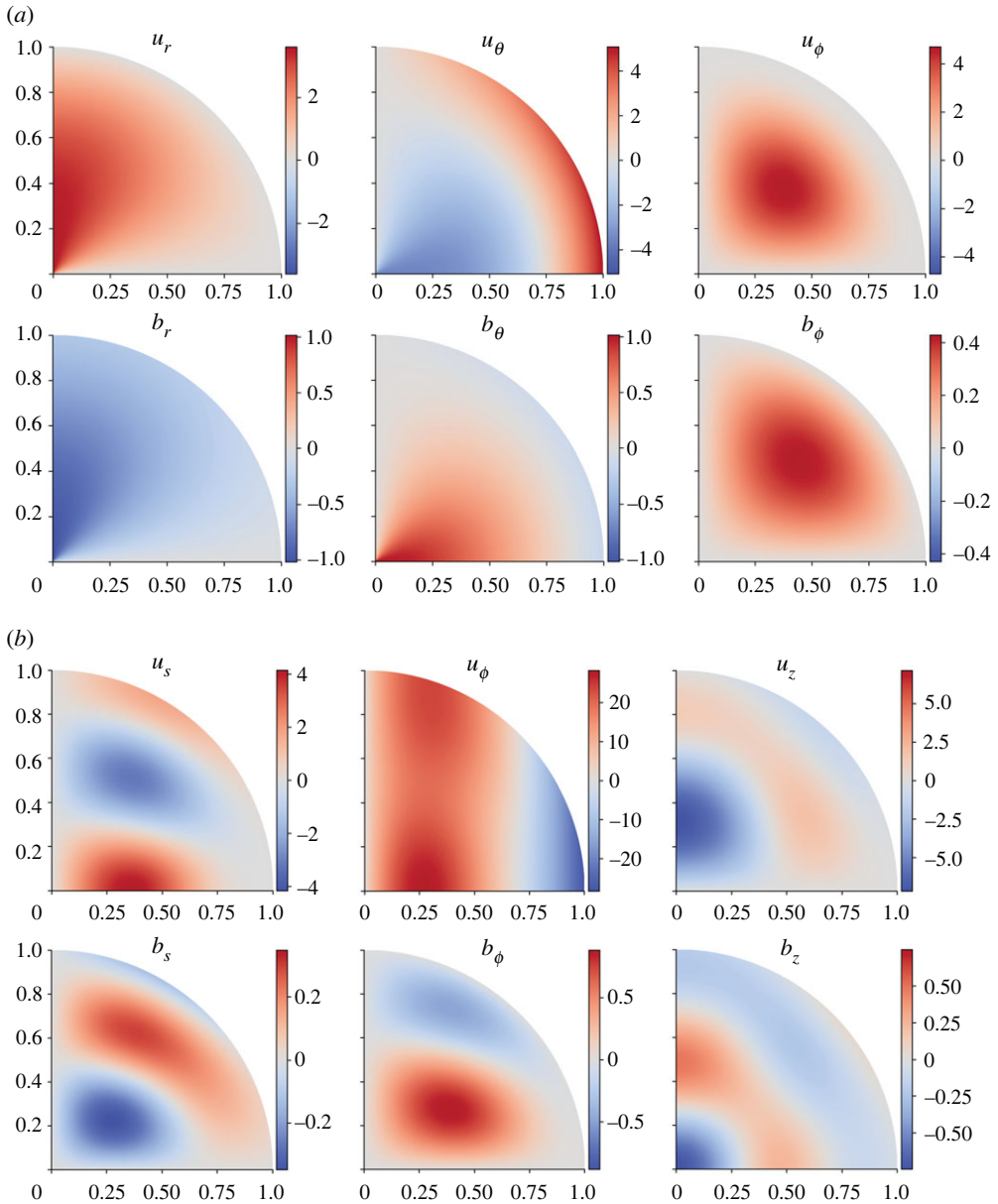


**Figure 15.** Two examples of axisymmetric MC modes for T1 and S1 configurations. (a) T1-E4. T1 configuration,  $m = 0$ ,  $\tilde{\omega} = -\pi^2$ . Both  $\mathbf{u}$  and  $\mathbf{b}$  are DP. (b) S1-E5. S1 configuration,  $m = 0$ ,  $\tilde{\omega} = -78.4 + 23.1i$ .  $\mathbf{u}$  is QP and  $\mathbf{b}$  is DP. Fields components of S1-E5 are shown in cylindrical coordinates. Both modes are computed at  $E_\eta = 10^{-9}$ ,  $\Lambda = 10$ ,  $L = 2N = 120$ . (Online version in colour.)

spectral method that gracefully handles all coordinate singularities present in a whole sphere geometry.

The magnetostrophic limit is in our opinion entirely respectable as we find  $E_\eta \rightarrow 0$  and  $E_\eta = 0$  are indistinguishable. Note that the former still allows the existence of fast modes, while the latter does not.

We find the pessimistic view of [19] to be unwarranted, as in a closed volume, there are no modes equivalent to the plane waves with wave vector perpendicular to  $\hat{\mathbf{z}}$ . The most dangerous modes are the quasi-geostrophic modes with small frequency (the numerator in the slow mode

dispersion relation), but those frequencies are finite and cannot vanish. Under the assumption of an axisymmetric background field, all modes are critically damped or overdamped. Thus, unlike the plane wave case, there are no occurrences of modes with large frequency and small decay rate.

We give evidence that the paradigm of westward propagation of columnar modes does not seem to be universal, and that eastward modes can also exist. Diffusion probably plays a role in facilitating this effect.

Our interest lies in computations of the geodynamo in the magnetostrophic regime, and it was with this goal that we developed the supporting results exposed here. A few provisos are in order, not least what the effects of non-zero background flows would be, and whether the results endure in the presence of non-axisymmetric background fields and the presence of an inner core.

**Data accessibility.** The normal modes calculated in this work are provided as electronic supplementary material documents.

**Authors' contributions.** J.L.: conceptualization, data curation, investigation, methodology, software, visualization, writing—original draft, writing—review and editing; P.M.: methodology, writing—review and editing; A.J.: conceptualization, funding acquisition, methodology, project administration, resources, supervision, writing—original draft, writing—review and editing.

All authors gave final approval for publication and agreed to be held accountable for the work performed therein.

**Conflict of interest declaration.** We declare we have no competing interests.

**Funding.** We are grateful for funding through an ETH research grant no. ETH-11 17-2 supporting the PhD of J.L. and from the European Research Council (agreement no. 833848-UEMHP) under the Horizon 2020 programme. Calculations made use of resources of the Swiss National Supercomputer Centre (CSCS) under account s1111, and we are grateful for the support received.

**Acknowledgements.** We thank Prof. Chris Jones for his interest and encouragement.

## Appendix A. The Malkus field

In this appendix, we treat the ideal diffusionless case where  $\nabla^2 \mathbf{b}$  is neglected. When  $\mathbf{B}_0$  is taken as the Malkus field (2.8), an analytical solution to the diffusionless version of (2.3) and (2.4) can be obtained. With the ansatz

$$\mathbf{u} = \tilde{\mathbf{u}} e^{im\phi + i\omega t} \quad \text{and} \quad \mathbf{b} = \tilde{\mathbf{b}} e^{im\phi + i\omega t}, \quad (\text{A } 1)$$

the normal mode problem was shown to be reducible to the pure inertial wave problem [8,9], with both  $\tilde{\mathbf{u}}$  and  $\tilde{\mathbf{b}}$  being inertial modes in the sphere related by

$$\tilde{\mathbf{b}} = \frac{m}{\omega} \tilde{\mathbf{u}}. \quad (\text{A } 2)$$

The canonical ideal problem is solved subject to  $u_r = b_r = 0$  at  $r = 1$ .

The frequency  $\omega$  is determined through a quadratic equation

$$E_\eta \omega^2 - \frac{1}{2} \omega_i \omega - \Lambda m(m - \omega_i) = 0, \quad (\text{A } 3)$$

in which  $\omega_i$  ( $-2 < \omega_i < 2$ ) is the inertial wave frequency defined by the following eigenvalue problem with non-penetration boundary condition (with time in units of  $\Omega^{-1}$ ).

$$i\omega_i \tilde{\mathbf{u}} + 2\hat{\mathbf{z}} \times \tilde{\mathbf{u}} + \nabla p = 0. \quad (\text{A } 4)$$

Equation (A 3) admits two solutions

$$\omega = \frac{1}{4} E_\eta^{-1} \omega_i \left( 1 \pm \sqrt{1 + \frac{16 E_\eta \Lambda m(m - \omega_i)}{\omega_i^2}} \right). \quad (\text{A } 5)$$

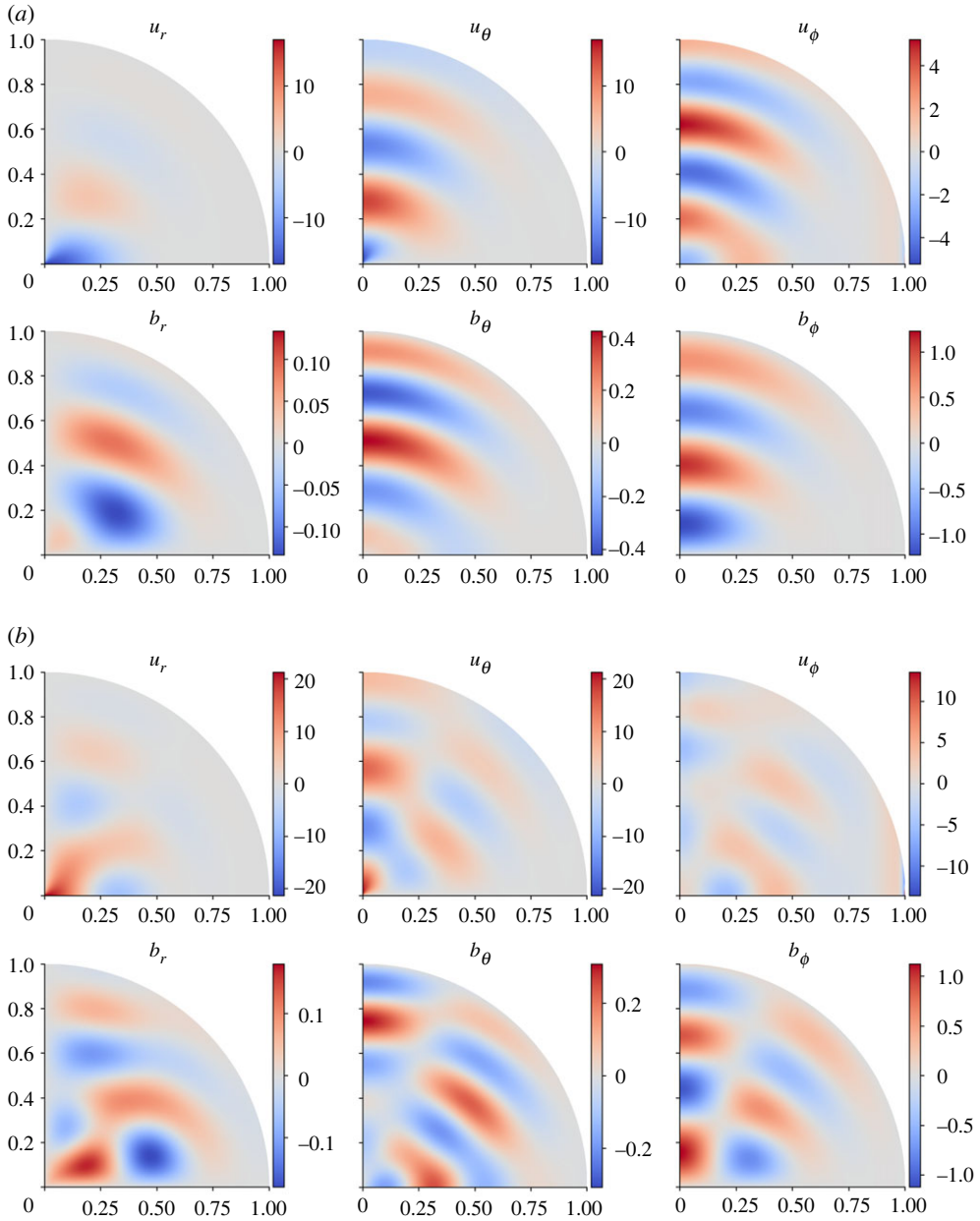


**Figure 16.** Normal modes in the S1 configuration. (a) S1-E1.  $m = 1$ ,  $\tilde{\omega} = -201.9 - 106.1i$ .  $\mathbf{u}$  is **QP**,  $\mathbf{b}$  is **DP**. (b) S1-E2.  $m = 1$ ,  $\tilde{\omega} = -287.9 - 115.2i$ .  $\mathbf{u}$  is **QP**,  $\mathbf{b}$  is **DP**. Both modes are computed at  $N = 60$ ,  $L = 120$ , with  $E_\eta = 10^{-9}$  and  $\Lambda = 1$ . (Online version in colour.)

Since the geophysically relevant regime is such that the magnetic Rossby number  $E_\eta$  is extremely small, two distinct branches emerge, namely a fast inertial-like branch

$$\omega \approx \frac{1}{2} E_\eta^{-1} \omega_i, \quad (\text{A } 6)$$

and a slow magnetic-like branch

$$\omega \approx -\frac{2\Lambda m(m - \omega_i)}{\omega_i}. \quad (\text{A } 7)$$

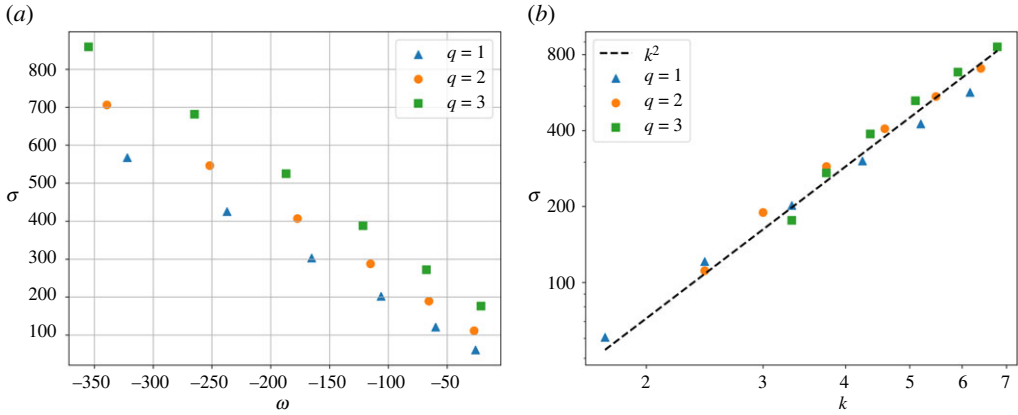


**Figure 17.** (a) Frequency  $\omega$  against decay rates  $\sigma$  for normal modes of  $1 \leq q \leq 3$  and  $1 \leq p \leq 6$  at  $m = 1$  of S1 configuration. (b) Decay rate  $\sigma$  plotted against wavenumber  $k = \sqrt{p^2 + q^2 + m^2}$ . The dashed line proportional to  $k^2$  is shown for reference. (Online version in colour.)

The  $\frac{1}{2}$  factor in (A 6) is due to our non-dimensionalization as the Coriolis term now is expressed as  $\hat{z} \times \mathbf{u}$  instead of  $2\hat{z} \times \mathbf{u}$  used for  $\omega_i$ . Note that the inertial branch has frequencies at  $O(E_\eta^{-1})$  while those of the magnetic-like branch are generally at  $O(1)$  or larger. Thus they are separated from each other in the eigen-spectrum of the system when  $E_\eta$  is small. Note that (A 6) and (A 7) are valid only under the assumption  $16E_\eta \Lambda m(m - \omega_i) \ll \omega_i^2$ .

The kinetic to magnetic energy ratio can be deduced using the relation (A 2)

$$\frac{E_{\text{kin}}}{E_{\text{mag}}} = E_\eta \frac{\tilde{u}^2}{\tilde{b}^2} = E_\eta \frac{\omega^2}{m^2}. \quad (\text{A } 8)$$

Approximations (A 6) and (A 7) for  $\omega$  show that, for  $\omega_i \sim O(1)$ , the inertial branch carries kinetic energy, while the magnetic branch is dominated by magnetic energy. When  $\omega_i^2 \approx 16E_\eta \Lambda m^2$  (e.g.  $\omega_i$  is  $O(E_\eta^{1/2})$  for small  $m$ ), (A 6) and (A 7) are no longer valid approximations of (A 5). These modes are in a regime where there is no clear separation between the ‘fast’ and ‘slow’ (though their signs are opposite for the Malkus case), and have roughly an equipartition between kinetic and magnetic energies. The analogy of this in Cartesian coordinates has been initially discussed by [2], and more recently by [49,50], which they named as inertial-Alfvén waves.

## Appendix B. Field controlled magneto–Coriolis modes in background field S1

We focus on the symmetry group in which  $\mathbf{b}$  is DP and  $\mathbf{u}$  is QP (thus labelled DP). The simple dipolar background field S1 allows interesting normal mode structures. The field lines of S1 field permit waves propagating along with them and also transverse to them. Let  $p$  be the wavenumber along  $\mathbf{B}_0$  and  $q$  be wavenumber of a direction transverse to  $\mathbf{B}_0$  in the meridional plane. It is then convenient to define the total wavenumber as

$$k = \sqrt{p^2 + q^2 + m^2}. \quad (\text{B } 1)$$

Figure 16a,b is two examples of such normal modes with  $p = 3, q = 1$  and  $p = 3, q = 2$ , respectively (we choose to determine  $p$  and  $q$  mainly according to the  $b_\phi$  component, and note that we start from one for  $q$ ). We are able to identify such modes for  $1 \leq q \leq 3$  and  $1 \leq p \leq 6$  at  $m = 1$ ; they travel eastward in the azimuthal direction. Similar branches can also be identified for  $m = 3$ . Although westward travelling modes with similar structures can be found, they do not seem to form complete branches ranging from small  $p$  to large  $p$ . Frequencies and decay rates of these modes

at  $m = 1$  are shown in figure 17a. Their decay rates follow the estimate of a scaling proportional to  $k^2$ .

## References

1. Gillet N, Jault D, Canet E, Fournier A. 2010 Fast torsional waves and strong magnetic field within the Earth's core. *Nature* **465**, 74–77. (doi:10.1038/nature09010)
2. Lehnert B. 1954 Magnetohydrodynamic waves under the action of the coriolis force. *Astrophys. J.* **119**, 647. (doi:10.1086/145869)
3. Lehnert B. 1955 Magnetohydrodynamic waves under the action of the coriolis force. II. *Astrophys. J.* **121**, 481. (doi:10.1086/146009)
4. Braginsky S. 1964 Magnetohydrodynamics of the Earth's core. *Geomag. Aeron.* **4**, 698–712.
5. Braginsky S. 1967 Magnetic waves in the Earth's core. *Geomag. Aeron.* **7**, 851–859.
6. Finlay C. 2008 Course 8 waves in the presence of magnetic fields, rotation and convection. In *Dynamos, Les Houches proceedings*, vol. 88 (eds P Cardin, LF Cugliandolo), pp. 403–450. Amsterdam, The Netherlands: Elsevier.
7. Finlay C. 2007 Magnetohydrodynamic waves. In *Encyclopedia of geomagnetism and paleomagnetism* (eds D Gubbins, HB Emilio), pp. 632–638. Berlin, Germany: Springer.
8. Greenspan H. 1968 *The theory of rotating fluids*. Cambridge, UK: Cambridge University Press.
9. Zhang K, Liao X. 1968 *Theory and modeling of rotating fluids: convection, inertial waves and precession*. Cambridge, UK: Cambridge University Press.
10. Moffatt K, Dormy E. 2019 *Self-exciting fluid dynamos*. Cambridge, UK: Cambridge University Press.
11. Steenbeck M, Krause F, Rädler K. 1966 Calculation of the average Lorentz field strength for an electrically conductive medium in turbulent motion influenced by Coriolis forces. *J. Nat. Res. A* **21**, 369–376.
12. Moffatt H. 1970 Dynamo action associated with random inertial waves in a rotating conducting fluid. *J. Fluid Mech.* **44**, 705–719. (doi:10.1017/S0022112070002100)
13. Krause F, Rädler K. 1980 *Mean-field hydrodynamics and dynamo theory*. Berlin, Germany: Akademie-Verlag.
14. Davidson P. 2014 The dynamics and scaling laws of planetary dynamos driven by inertial waves. *Geophys. J. Int.* **198**, 1832–1847. (doi:10.1093/gji/ggu220)
15. Davidson P, Ranjan A. 2015 Planetary dynamos driven by helical waves—II. *Geophys. J. Int.* **202**, 1646–1662. (doi:10.1093/gji/ggv232)
16. Davidson P. 2016 Dynamos driven by helical waves: scaling laws for numerical dynamos and for the planets. *Geophys. J. Int.* **207**, 680–690. (doi:10.1093/gji/ggw297)
17. Davidson P, Ranjan A. 2018 Are planetary dynamos driven by helical waves? *J. Plasma Phys.* **84**, 735840304. (doi:10.1017/S0022377818000466)
18. Taylor J. 1963 The magneto-hydrodynamics of a rotating fluid and the Earth's dynamo problem. *Proc. R. Soc. Lond. A.* **274**, 274–283. (doi:10.1098/rspa.1963.0130)
19. Walker M, Barenghi C, Jones C. 1998 A note on dynamo action at asymptotically small Ekman number. *Geophys. Astrophys. Fluid Dyn.* **88**, 261–275. (doi:10.1080/03091929808245476)
20. Kuang W, Bloxham J. 1999 Numerical modeling of magnetohydrodynamic convection in a rapidly rotating spherical shell: weak and strong field dynamo action. *J. Comput. Phys.* **153**, 51–81. (doi:10.1006/jcph.1999.6274)
21. Hollerbach R. 2003 The range of timescales on which the geodynamo operates. In *Earth's core: dynamics, structure, rotation* (eds V Dehant, KC Creager, S Karato, S Zatman), pp. 181–192. New York, NY: Wiley.
22. Wood TS, McIntyre ME. 2011 Polar confinement of the Sun's interior magnetic field by laminar magnetostrophic flow. *J. Fluid Mech.* **677**, 445–482. (doi:10.1017/jfm.2011.93)
23. Roberts PH, Wu CC. 2014 On the modified Taylor constraint. *Geophys. Astrophys. Fluid Dyn.* **108**, 696–715. (doi:10.1080/03091929.2014.942955)
24. Hide R. 1966 Free hydromagnetic oscillations of the Earth's core and the theory of the geomagnetic secular variation. *Phil. Trans. R. Soc. Lond. A* **259**, 615–647. (doi:10.1098/rsta.1966.0026)
25. Jault D, Finlay C. 2015 Waves in the core and mechanical core-mantle interactions. In *Treatise on Geophysics: Core Dynamics* (ed. G Schubert), pp. 225–245. Amsterdam, The Netherlands: Elsevier.

26. Canet E, Finlay CC, Fournier A. 2014 Hydromagnetic quasi-geostrophic modes in rapidly rotating planetary cores. *Phys. Earth Planet. Inter.* **229**, 1–15. (doi:10.1016/j.pepi.2013.12.006)
27. Hori K, Jones C, Teed R. 2015 Slow magnetic Rossby waves in the Earth's core. *Geophys. Res. Lett.* **42**, 6622–6629. (doi:10.1002/2015GL064733)
28. Hori K, Teed R, Jones C. 2018 The dynamics of magnetic Rossby waves in spherical dynamo simulations: a signature of strong-field dynamos? *Phys. Earth Planet. Inter.* **276**, 68–85. (doi:10.1016/j.pepi.2017.07.008)
29. Malkus WV. 1967 Hydromagnetic planetary waves. *J. Fluid Mech.* **28**, 793–802. (doi:10.1017/S0022112067002447)
30. Luo J, Jackson A. 2022 Waves in the Earth's core. I. Mildly diffusive torsional oscillations. *Proc. R. Soc. A* **478**, 20210982. (doi:10.1098/rspa.2021.0982)
31. Schmitt D. 2010 Magneto-inertial waves in a rotating sphere. *Geophys. Astrophys. Fluid Dyn.* **104**, 135–151. (doi:10.1080/03091920903439746)
32. Schmitt D. 2012 Quasi-free-decay magnetic modes in planetary cores. *Geophys. Astrophys. Fluid Dyn.* **106**, 660–680. (doi:10.1080/03091929.2012.681306)
33. Acheson D, Hide R. 1973 Hydromagnetics of rotating fluids. *Rep. Prog. Phys.* **36**, 159–221. (doi:10.1088/0034-4885/36/2/002)
34. Jackson A. 2003 Intense equatorial flux spots on the surface of the Earth's core. *Nature* **424**, 760–763. (doi:10.1038/nature01879)
35. Zhang K, Earnshaw P, Liao X, Busse F. 2001 On inertial waves in a rotating fluid sphere. *J. Fluid Mech.* **437**, 103–119. (doi:10.1017/S0022112001004049)
36. Worland SJ. 2004 Magnetoconvection in rapidly rotating spheres. PhD thesis, University of Exeter.
37. Livermore PW, Jones CA, Worland SJ. 2007 Spectral radial basis functions for full sphere computations. *J. Comput. Phys.* **227**, 1209–1224. (doi:10.1016/j.jcp.2007.08.026)
38. Marti P *et al.* 2014 Full sphere hydrodynamic and dynamo benchmarks. *Geophys. J. Int.* **197**, 119–134. (doi:10.1093/gji/ggt518)
39. Marti P, Jackson A. 2016 A fully spectral methodology for magnetohydrodynamic calculations in a whole sphere. *J. Comput. Phys.* **305**, 403–422. (doi:10.1016/j.jcp.2015.10.056)
40. Marti P, Jackson A. 2021 Accurate and efficient Jones-Worland spectral transforms for planetary applications. In *Proc. of the Platform for Advanced Scientific Computing Conference*, article 16, pp. 1–10. New York, NY: ACM.
41. Boyd J. 2001 *Chebyshev and fourier spectral methods*. New York, NY: Dover Publications Inc.
42. Gubbins D, Zhang K. 1993 Symmetry properties of the dynamo equations for palaeomagnetism and geomagnetism. *Phys. Earth Planet. Inter.* **75**, 225–241. (doi:10.1016/0031-9201(93)90003-R)
43. Livermore PW, Ierley G, Jackson A. 2009 The construction of exact Taylor states. I: the full sphere. *Geophys. J. Int.* **179**, 923–928. (doi:10.1111/j.1365-246X.2009.04340.x)
44. Labbé F, Jault D, Gillet N. 2015 On magnetostrophic inertia-less waves in quasi-geostrophic models of planetary cores. *Geophys. Astrophys. Fluid Dyn.* **109**, 587–610. (doi:10.1080/03091929.2015.1094569)
45. Jackson A, Maffei S. 2020 Plesio-geostrophy for Earth's core: I. Basic equations, inertial modes and induction. *Proc. R. Soc. A* **476**, 20200513. (doi:10.1098/rspa.2020.0513)
46. Gerick F, Jault D, Noir J. 2021 Fast quasi-geostrophic magneto-Coriolis modes in the Earth's core. *Geophys. Res. Lett.* **48**, e2020GL090803. (doi:10.1029/2020GL090803)
47. Triana SA, Trinh A, Requier J, Zhu P, Dehant V. 2021 The viscous and Ohmic damping of the Earth's free core nutation. *J. Geophys. Res. Solid Earth* **126**, e2020JB021042. (doi:10.1029/2020JB021042)
48. Lin Y, Ogilvie GI. 2018 Tidal dissipation in rotating fluid bodies: the presence of a magnetic field. *Mon. Not. R. Astron. Soc.* **474**, 1644–1656. (doi:10.1093/mnras/stx2764)
49. Bardsley O, Davidson PA. 2016 Inertial-Alfvén waves as columnar helices in planetary cores. *J. Fluid Mech.* **805**, R2. (doi:10.1017/jfm.2016.577)
50. Bardsley O, Davidson PA. 2017 The dispersion of magnetic-Coriolis waves in planetary cores. *Geophys. J. Int.* **210**, 18–26. (doi:10.1093/gji/ggx143)